Remote Sensing and hydrological modeling of the Upper Bhima catchment

Draft

W.W. Immerzeel
A. Gaur
P. Droogers

NIVR
Nederlands Instituut voor Vliegtuigontwikkeling en Ruimtevaart
Netherlands Agency for Aerospace Programmes

Research paper no. 3

IWMI International Water Management Institute

Future Water Science for Solutions

P.O. Box 35
2600 AA Delft
The Netherlands
Kluyverweg 1
2629 HS Delft
The Netherlands
Tel. +31 (0)15 278 80 25
Fax +31 (0)15 262 30 96
Email info@nivr.nl
www.nivr.nl

NATIONAL USER SUPPORT PROGRAMME (NUSP) 2001-2005

http://www.ao-go.nivr.nl

The National User Support Programme 2001-2005 (NUSP) is executed by the Netherlands Agency for Aerospace Programmes (NIVR) and the Space Research Organization of the Netherlands (SRON). The NUSP is financed from the national space budget. The NUSP subsidy arrangement contributes to the development of new applications and policy-supporting research, institutional use and use by private companies.

The objectives of the NUSP are:

- To support those in the Netherlands, who are users of information from existing and future European and non-European earth observation systems in the development of new applications for scientific research, industrial and policy research and operational use;

- To stimulate the (inter)national service market based on space-based derived operational geo-information products by means of strengthening the position of the Dutch private service sector;

- To assist in the development of a national Geo-spatial data and information infrastructure, in association with European and non-European infrastructures, based on Dutch user needs;

- To supply information to the general public on national and international space-based geo-information applications, new developments and scientific research results.

Remote Sensing and hydrological modeling of the Upper Bhima catchment

Authors: W. Immerzeel (FutureWater)
A. Gaur (IWMI)
P. Droogers (FutureWater)

This research was funded by: NIVR/SRON/NWO User Support Programme 2

Generaal Foulkesweg 28 ● 6703 BS Wageningen ● Tel: 0317-460050
E-mail: info@futurewater.nl ● Website: www.futurewater.nl

Preface

This report contributes to a research project undertaken by FutureWater entitled: "Remotely Sensed based hydrological model calibration for basin scale water resources planning: embedding case for Krishna Basin, India" (GO-2005/025). This project is financially supported by NIVR (Nederlands Instituut voor Vliegtuigontwikkeling en Ruimtevaart) in the context of "Tijdelijke subsidieregeling Nationaal Programma Gebruikers Onderstuining (GO).

The report describes the use of Remote Sensing in hydrological modeling of the Upper Bhima catchment.

FutureWater
Generaal Foulkesweg 28
6703 BS Wageningen
tel: 0317 460050
email: info@futurewater.nl

Table of contents

1 Introduction

2 Soil and Water Assessment Tool

2.1 Background

SWAT[1] was developed primarily by the United States Department of Agriculture (USDA) to predict the impact of land management practices on water, sediment and agricultural chemical yields in large complex watersheds with varying soils, land use and management conditions over long periods of time. The SWAT model has been extensively used, is in the public domain and can be considered as becoming the de-facto standard in spatial decision support systems.

SWAT represents all the components of the hydrological cycle including: rainfall, snow, snow-cover and snow-melt, interception storage, surface runoff, up to 10 soil storages, infiltration, evaporation, evapotranspiration, lateral flow, percolation, pond and reservoir water balances, shallow and deep aquifers, channel routing. It also includes irrigation from rivers, shallow and deep groundwater stores, ponds/reservoirs and rivers, transmission losses and irrigation onto the soil surface. It includes sediment production based on a modified version of the Universal Loss Equation and routing of sediments in river channels. SWAT tracks the movement and transformation of several forms of nitrogen and phosphorus in the watershed. It also tracks the movement and decay of pesticides. All include channel routing components and carrying of pollutants by sediments. SWAT has a modular set-up and it goes beyond the scope of this report to get into detail on each of these modules, but reference is made to the theoretical documentation (Neitsch et al, 2001).

For modeling purposes, a watershed may be partitioned into a number of sub-watersheds or sub-basins. The use of sub-basins in a simulation is particularly beneficial when different areas of the watershed are dominated by land uses or soils dissimilar enough in properties to impact hydrology. By partitioning the watershed into sub-basins, the user is able to reference different areas of the watershed to one another spatially. Input information for each sub-basin is grouped or organized into the following categories: climate; hydrologic response units or HRUs; ponds/wetlands; groundwater; and the main channel, or reach, draining the sub-basin. Hydrologic response units are lumped land areas within the sub-basin that are comprised of unique land cover, soil, and management combinations.

No matter what type of problem studied with SWAT, the water balance is the driving force behind everything that happens in the watershed. To accurately predict the movement of pesticides, sediments or nutrients, the hydrologic cycle as simulated by the model must conform to what is happening in the watershed. Simulation of the hydrology of a watershed can be separated into two major divisions. The first division is the land phase of the hydrologic cycle, depicted in Figure 1. The land phase of the hydrologic cycle controls the amount of water, sediment, nutrient and pesticide loadings to the main channel in each sub-basin.

[1] http://www.brc.tamus.edu/swat/index.html

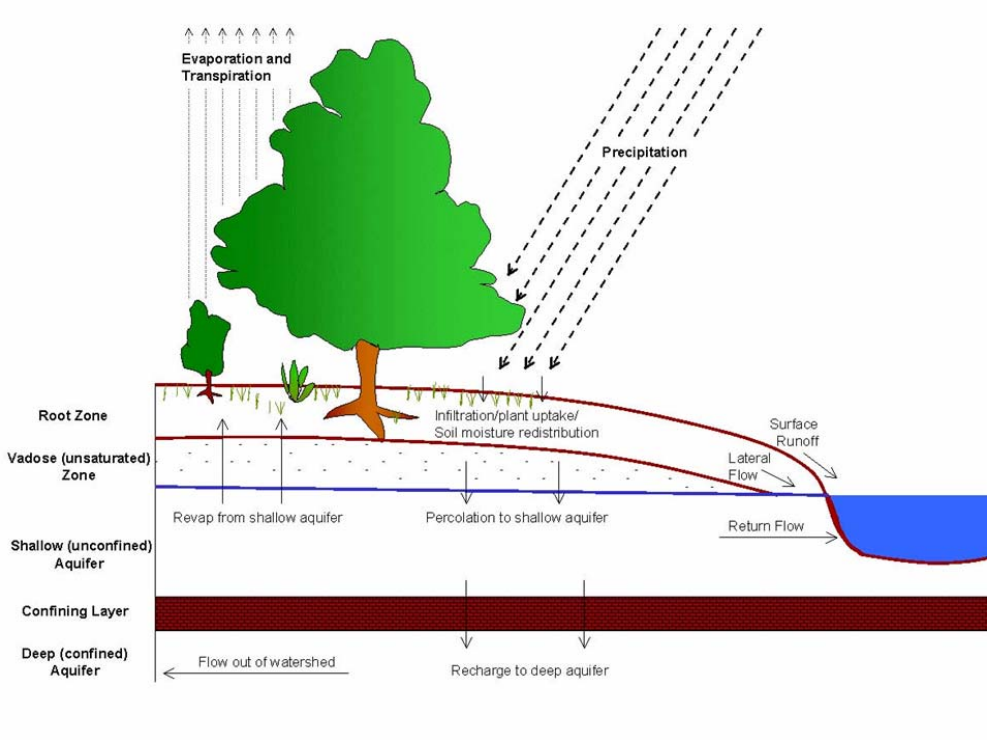

Figure 1: Water balance SWAT.

The second division is the water or routing phase of the hydrologic cycle which can be defined as the movement of water, sediments, etc. through the channel network of the watershed to the outlet.
Once SWAT determines the loadings of water, sediment, nutrients and pesticides to the main channel, the loadings are routed through the stream network of the watershed using a command structure. In addition to keeping track of mass flow in the channel, SWAT models the transformation of chemicals in the stream and streambed.

2.2 Evaporation

Evapotranspiration is a collective term for all processes by which water in the liquid or solid phase at or near the earth's surface becomes atmospheric water vapor. Evapotranspiration includes evaporation from rivers and lakes, bare soil, and vegetative surfaces; evaporation from within the leaves of plants (transpiration); and sublimation from ice and snow surfaces. The model computes evaporation from soils and plants separately as described by Ritchie (1972). Potential soil water evaporation is estimated as a function of potential evapotranspiration and leaf area index (area of plant leaves relative to the area of the HRU). Actual soil water evaporation is estimated by using exponential functions of soil depth and water content. Plant transpiration is simulated as a linear function of potential evapotranspiration and leaf area index. Potential evapotranspiration is the rate at which evapotranspiration would occur from a large area completely and uniformly covered with growing vegetation which has access to an unlimited supply of soil water. This rate is assumed to be unaffected by micro-climatic processes such as advection or heat-storage effects. The model offers three options

for estimating potential evapotranspiration: Hargreaves (Hargreaves et al., 1985), Priestley-Taylor (Priestley and Taylor, 1972), and Penman-Monteith (Monteith, 1965).

2.3 Crop growth

For each day of simulation, potential plant growth, i.e. plant growth under ideal growing conditions is calculated. Ideal growing conditions consist of adequate water and nutrient supply and a favorable climate. The biomass production functions are to a large extend similar to SEBAL; First the Absorbed Photosynthetical Radiation (APAR) is computed from intercepted solar radiation as a function of LAI, followed by a Light Use Efficiency (LUE) that is in SWAT essentially a function of carbon dioxide concentrations and vapor pressure deficits. Whilst LAI is simulated in SWAT, the fractional Photosynthetical Active Radiation (fPAR) is measured in SEBAL. The crop yield is computed as the harvestable fraction of the accumulated biomass production across the growing season.

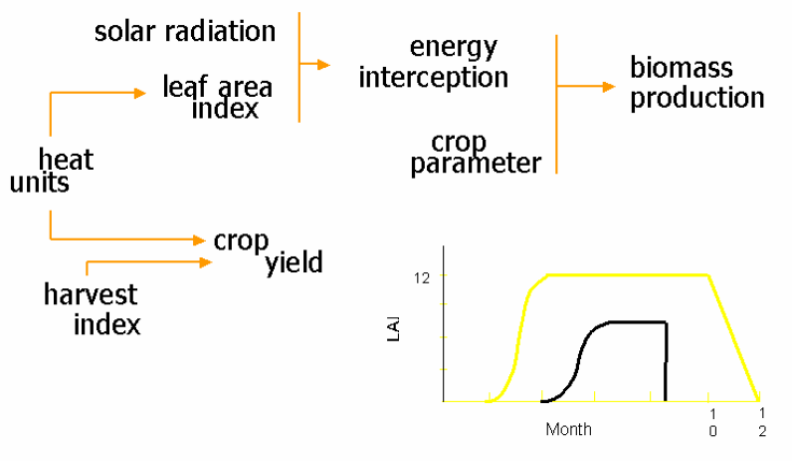

Figure 2: Parameterization of crop production processes for estimating crop yiel

2.4 Irrigation

Irrigation may be scheduled manually or applied automatically by the model as response to a water deficit in the soil. Irrigation water applied to a sub basin is obtained from one of five types of water sources: a reach, a reservoir, a shallow aquifer, a deep aquifer, or a source outside the watershed. For this study it is assumed that all water originated from the shallow aquifer. If automatic irrigation is applied all soil layers are filled up to field capacity. If manually scheduling is used all scheduled water is applied and potential excess water percolates to the shallow aquifer. In this study irrigation water is applied automatically based on a predefined water stress criterion per sub basin. Water stress is 0.0 under optimal water conditions and approaches 1.0 as the soil water conditions vary from the optimal. Water stress is simulated by comparing actual and potential plant transpiration:

$$wstrs = 1 - \frac{E_{t,act}}{E_t} = 1 - \frac{w_{actualup}}{E_t}$$

where wstrs is the water stress for a given day, Et is the maximum plant transpiration on a given day (mm H2O), Et,act is the actual amount of transpiration on a given day (mm H2O) and wactualup is the total plant water uptake for the day (mm H2O). The water stress criterion is used in calibrating simulated Et,act with the measured SEBAL Et,act.

2.5 *Groundwater*

Recharge to unconfined aquifers occurs via percolation of excessively wet root zones. Recharge to confined aquifers by percolation from the surface occurs only at the upstream end of the confined aquifer, where the geologic formation containing the aquifer is exposed at the earth's surface, flow is not confined, and a water table is present. River courses and irrigation canals are connected to the groundwater system, and surface water – groundwater interactions are taken care for.
After water is infiltrated into the soil, it can basically leave again the ground as lateral flow from the upper soil layer – which mimics a 2D flow domain in the unsaturated zone – or from return flow that leaves the shallow aquifer and drains into a nearby river. The remaining part of the soil moisture can feed into the deep aquifer, from where it can be pumped back by means of artificial extraction. The total return flow thus consists of surface runoff, lateral outflow from root zone and aquifer drainage to river.

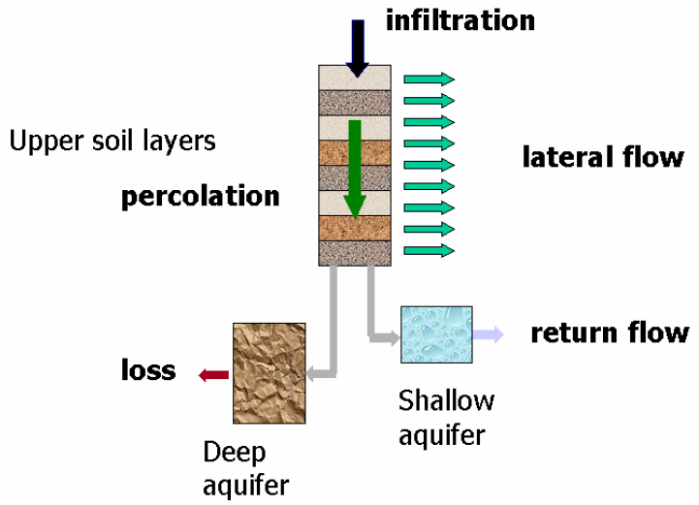

Figure 3: Schematic diagram of the partitioning of infiltration into sub-surface water fluxes after water uptake by roots have taken place

SWAT simulates two aquifers in each subbasin. The shallow aquifer is an unconfined aquifer that contributes to flow in the main channel or reach of the subbasin. The deep aquifer is a confined aquifer. Water that enters the deep aquifer is assumed to contribute to streamflow somewhere outside of the watershed (Arnold et al., 1993). The effects of groundwater extractions on baseflow (Q_{gw}), defined as the contribution of the shallow aquifer to stream flow, is of specific relevance in this study.

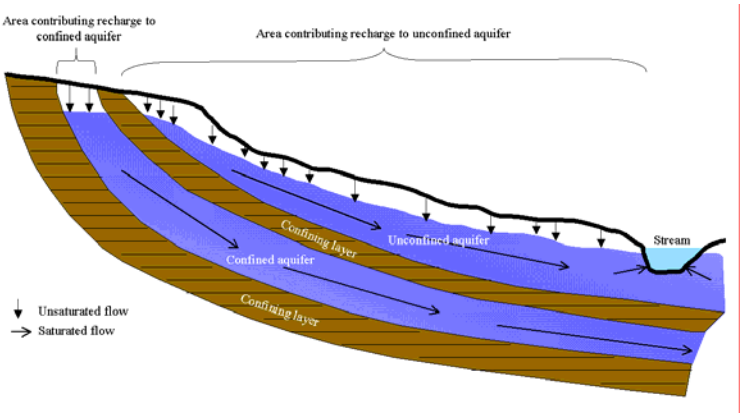

Figure 4: Schematic representation of shallow and deep aquifers in SWAT (Neitsch et al, 2001)

Base flow calculations are based on a combination of Hooghoudt (1940) and Smedema and Rycroft (1983) according to

$$Q_{gw,i} = Q_{gw,i-1} \cdot \exp\left[-\alpha_{gw} \cdot \Delta t\right] + w_{rchrg,sh} \cdot \left(1 - \exp\left[-\alpha_{gw} \cdot \Delta t\right]\right)$$

where $Q_{gw,i}$ is the groundwater flow into the main channel on day i (mm H_2O), $Q_{gw,i-1}$ is the groundwater flow into the main channel on day i-1 (mm H_2O), α_{gw} is the baseflow recession constant, Δt is the time step (1 day), $w_{rchrg,sh}$ is the amount of recharge entering the shallow aquifer on day i (mm H_2O). To enable the simulation of the effect of groundwater extractions a component was added to the model which assumes a minimal baseflow defined as a percentage of the actual amount of water stored in the aquifer. For calculations of water table fluctuations a specific yield is assumed of 0.15 m^3/m^3 is assumed.

2.6 Reservoirs

Reservoirs are located within a sub basin off the main channel. Water flowing into these water bodies must originate from the sub basin in which the water body is located. Reservoirs are located on the main channel network. They receive water from all sub basins upstream of the water body. A schematic representation of reservoirs in SWAT is shown in Figure 5.

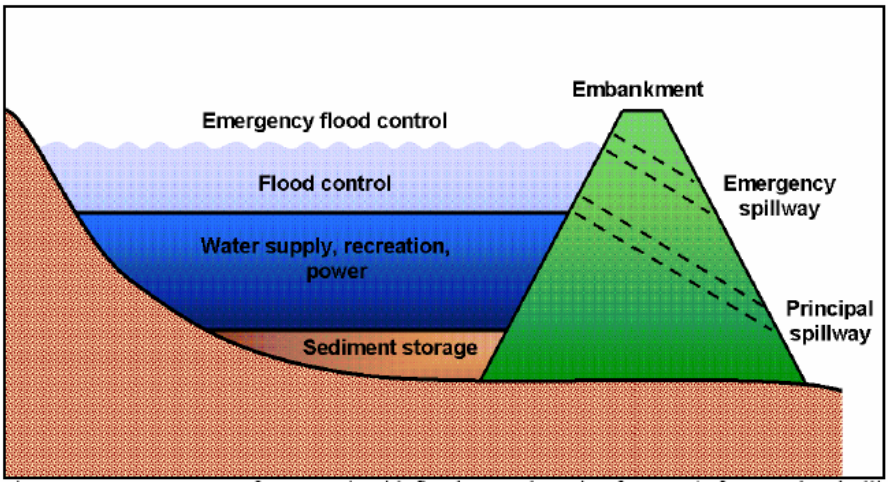

Figure 5: Schematic representation reservoirs in SWAT (Neitsch et al, 2001)

The water balance for reservoirs includes inflow, outflow, rainfall on the surface, evaporation, seepage from the reservoir bottom and diversions.

The model offers three alternatives for estimating outflow from the reservoir. The first option allows the user to input measured outflow. The second option, designed for small, uncontrolled reservoirs, requires the users to specify a water release rate. When the reservoir volume exceeds the principle storage, the extra water is released at the specified rate. Volume exceeding the emergency spillway is released within one day. The third option, designed for larger, managed reservoirs, has the user specify monthly target volumes for the reservoir.

3 Land use classification

3.1 Introduction

Based on a study for the entire Krishna basin a land use map was available at the start of the project. This land use map (Figure 6) was derived from a temporal series of MODIS[2] Normalized Difference Vegetation Index (NDVI) data. The first results of the evaporation mapping revealed however that the land use map was not accurate enough, specifically in the irrigated areas and the forested areas in the Western Ghats. The Upper Bhima sub-basin has a number of specific characteristics which caused errors in the land use classification.

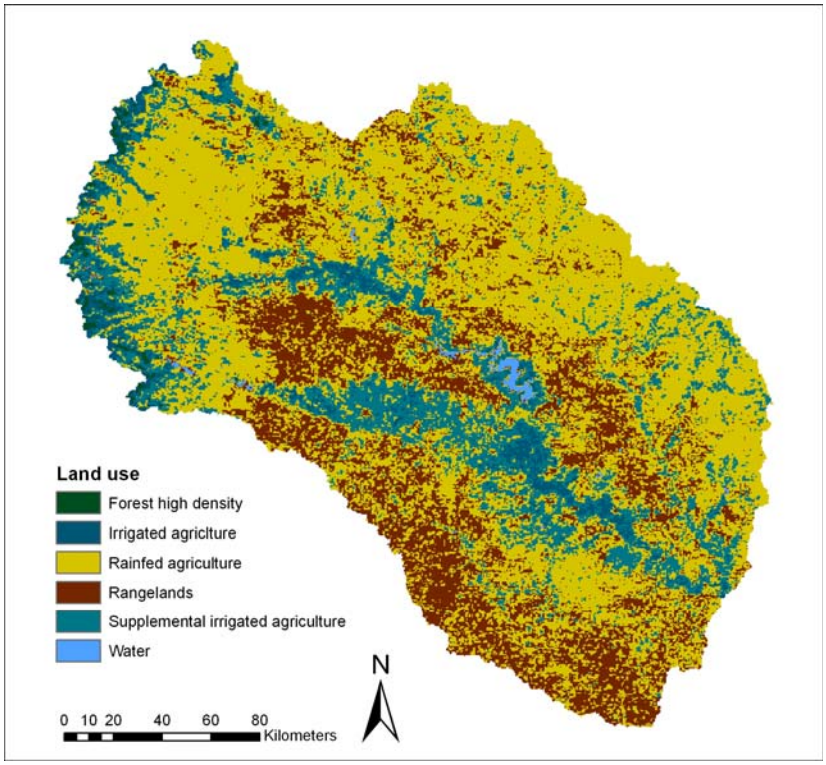

Figure 6 Land use map based on Krishna basin classification

First of all the acreage of irrigated agriculture seems to be underestimated. The command areas of the Khadakwasla, Ujani and Yadgaon and Bhatghar reservoirs are mainly cultivated with sugarcane. Sugar cane is a C4 crop, produces large amounts of biomass with yields up 70 t/ha. The growing season of sugarcane has length of 11 months and sugar cane can thus be grown year around. These unique properties might have led to an inaccurate representation of the sugarcane areas. Secondly there seems to be large areas in and around the Western Ghats which are classified as rain fed agriculture but in practice they should be classified as low density forests.

[2] http://modis.gsfc.nasa.gov/

Because of these errors a new land use classification has been performed for the Upper Bhima sub basin. This chapter describes the methodology used and the results of the land use classification.

3.2 Remote Sensing and land use classification

The application of Remote Sensing is a common technique in land use and land cover (LULC) mapping. Traditionally multi-spectral data are used to classify pixels in the image as a certain LULC unit. The basic assumption being that each LULC unit exhibits unique spectral behavior. A LULC has unique reflectance and emittance properties at different location along the electromagnetic spectrum. This is illustrated in Figure 7. It shows the spectra of water, bare soil and vegetation and the bands of the Landsat TM satellite. The combination of digital numbers (DN) for each band for each pixel allows the classification of the pixel to a certain land use class. This technique is summarized as spectral pattern recognition.

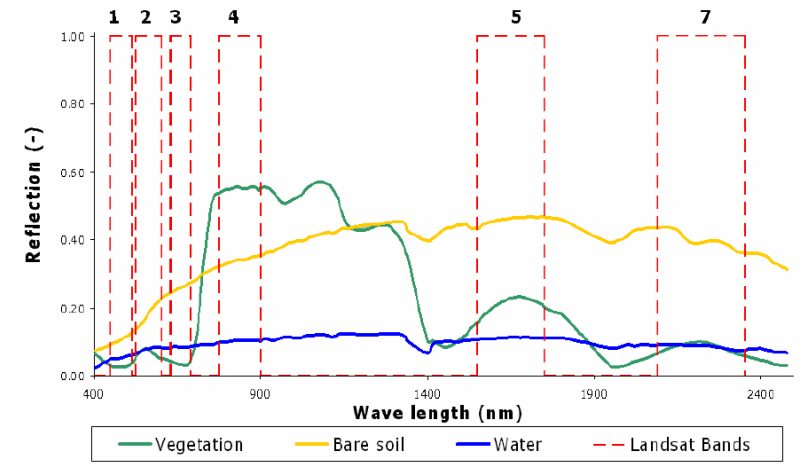

Figure 7: Spectral behaviour of major land uses and the spectral bands of the Landsat satellite

Multi-spectral image classification is usually performed using one or a limited number of images. In agricultural areas however there may be distinct spectral and spatial changes during the growing season which necessitates the use of multi-temporal imagery. A single image at the onset of the growing would prohibit the distinction between bare soil and a crop. Problems may also arise when dual-cropping patterns are prevalent. Winter wheat in fall may show a similar spectrum as a pasture in spring. If imagery of multiple dates are used the chances on erroneous classifications are much less (Immerzeel and Droogers, 2005, Bastiaanssen *et al.*, 2006)

There is a distinction between supervised and unsupervised classification techniques (Lillesand and Kiefer, 2000).

In a supervised classification the spectral signatures of training areas with known LULC are specified to the classification algorithm. After the training stage the actual classification process can take place. During the classification process each pixel is compared to the specified spectral signatures and labelled to the corresponding LULC class. There are four popular classification methods which are commonly used:

- The Box classifier method
- The Minimum Distance classifier
- The Minimum Mahalanobis Distance classifier
- The Maximum Likelihood classifier

The Box classifier method is based on the distances towards class means and the standard deviation per band of each class. Multi-dimensional boxes are drawn around class means based on the standard deviation of each class. The user can insert a multiplication factor (usually > 1) to make all boxes a bit wider. If the spectral values of a pixel to be classified fall inside a box, then that class name is assigned. If the spectral values of a pixel fall within two boxes, the class name of the box with the standard deviation is assigned. If the spectral values of a pixel do not fall within a box, the undefined value is assigned. The default multiplication factor is the square root of √3 for 3 bands.

The Minimum Distance classifier is based on the Euclidean distances towards class means only. For the spectral values of a pixel to be classified, the distances towards the class means are calculated. If the shortest (Euclidean) distance to a class mean is smaller than the user-defined threshold, then this class name is assigned to the output pixel. Else the undefined value is assigned.

For the spectral values of a pixel to be classified with the Minimum Mahalanobis Distance classifier, the distances towards the class means are calculated as Mahalanobis distance, which depends on the distances towards class means and the variance-covariance matrix of each class. The class name with the shortest Mahalanobis distance is assigned, if this distance is smaller than the user-defined threshold value. Else, the undefined value is assigned.

The Maximum Likelihood classification assumes that spectral values of training pixels are statistically distributed according to a multi-variate normal probability density function. For each set of spectral input values, the distance is calculated towards each of the classes is calculated using Mahalanobis distance. Another factor is added to compensate for within class variability. The class name with the shortest distance is assigned, if this distance is smaller than the user-defined threshold value. Else, the undefined value is assigned.

In an unsupervised classification the image data are first of classified by aggregating them into spatial clusters based on the statistical properties of the pixel values (e.g. average and variation). The number of clusters is usually chosen larger then the actual number of LULC classes which are expected. After the clustering the LULC identity is assigned to each land use class based on ground reference data, which is usually not an easy task. In case of the unsupervised classification the classification step is followed by the training step. The clusters are natural groupings of pixels with similar spectral behavior. There are numerous clustering algorithms that can determine these natural groupings. One common form of clustering is called the K-means approach. The user identifies the number of clusters to be located in the image. The algorithm then randomly locates the number of specified cluster centers in the multidimensional feature space. Each pixel is then assigned to the cluster whose arbitrary mean vector is closest. After all pixels are classified revised mean vectors for each cluster is calculated and the process is iteratively repeated until no significant changes in the location of the mean vectors occur. The convergence criterion used to stop the iteration is specified by the user.
Other commonly used methods are based on textural information of the image. They use information from neighboring pixels to assign classes to pixels and are referred to as contextual classifiers.

Spectral rationing is another important technique that can support image classifications. It refers to an enhancement technique by combining pixel values from different bands. The most commonly used ratio techniques are ratios to enhance the vegetation cover such as the Normalized Difference Vegetation Index (NDVI). The NDVI is defined as:

$$NDVI = \frac{NIR - RED}{NIR + RED} \qquad \text{Eq. 1}$$

Where NIR is the reflectance in the near infra-red part of the spectrum (wavelength = 0.7-1.1 µm) and RED is the reflectance in the red part of the spectrum (wavelength = 0.6-0.7 µm). Healthy vegetation free of environmental stress reflects well in the NIR part of the spectrum and reflects poorly in the red part of the spectrum. The NDVI amplifies this effect.

In this study a combination of spectral rationing and multi-temporal unsupervised classification is applied to make a land use classification of the Upper Bhima sub basin. A time series of 16 NDVI images acquired with the Moderate Resolution Imaging Spectroradiometer (MODIS) is used to perform an unsupervised classification.

3.3 MODIS[3]

MODIS is a key instrument aboard the Terra (EOS AM) and Aqua (EOS PM) satellites. Terra's orbit around the Earth is timed so that it passes from north to south across the equator in the morning, while Aqua passes south to north over the equator in the afternoon. Terra was launched on December 18 1999 and Aqua was launched on May 4 2002. These data will improve the understanding of global dynamics and processes occurring on the land, in the oceans, and in the lower atmosphere. MODIS is playing a vital role in the development of validated, global, interactive Earth system models able to predict global change accurately enough to assist policy makers in making sound decisions concerning the protection of our environment.

The MODIS instrument provides high radiometric sensitivity (12 bit) in 36 spectral bands ranging in wavelength from 0.4 µm to 14.4 µm. The responses are custom tailored to the individual needs of the user community and provide exceptionally low out-of-band response. Two bands are imaged at a nominal resolution of 250 m at nadir, with five bands at 500 m, and the remaining 29 bands at 1 km. A ±55-degree scanning pattern at the EOS orbit of 705 km achieves a 2,330-km swath and provides global coverage every one to two days.
In this study the MOD02 product acquired with the Aqua satellite is used. The Level 1B data set contains calibrated and geolocated at-aperture radiances for 36 bands generated from MODIS Level 1A sensor counts (MOD 01). The radiances are in W/(m2 µm sr). The NDVI is calculated using band 1 (620-670 nm) and band 2 (841-876 nm) which both have a spatial resolution of 250 meter:

$$NDVI_{MODIS} = \frac{band2 - band1}{band2 + band1}$$

[3] http://modis.gsfc.nasa.gov/index.php

3.4 Classification of the Upper Bhima sub basin

In this study a time series of 16 cloud free MODIS AQUA NDVI images is used from October 2004 to May 2005. Due to the monsoon cloud free images from June to September could not be obtained. The dates and time of acquisition of the images used are shown in Table 1.

Image #	Date	Acquisition time (GMT)	
		Hour	Minute
1	16/10/2004	8	10
2	21/10/2004	8	30
3	04/11/2004	8	40
4	22/11/2004	8	30
5	03/12/2004	8	10
6	17/12/2004	8	20
7	07/01/2005	8	40
8	18/01/2005	8	20
9	12/02/2005	8	15
10	19/02/2005	8	20
11	14/03/2005	8	30
12	23/03/2005	8	20
13	10/04/2005	8	10
14	19/04/2005	8	5
15	14/05/2005	7	55
16	17/05/2005	8	25

Table 1: Acquisition dates and time of MODIS imagery. Local time in the Upper Bhima catchment is GMT +5:30

The 16 NDVI images which were used in the classification are shown in Figure 8. The NDVI peak is clearly just after the monsoon in October and for the major part of the sub basin the NDVI gradually decreases except for the forested parts in the Western Ghats and the irrigated areas downstream of the main reservoirs (Khadakwasla, Ujani and Yadgaon and Bhatghar). Just before the onset of the monsoon by the end of May the NDVI is lowest in the basin.

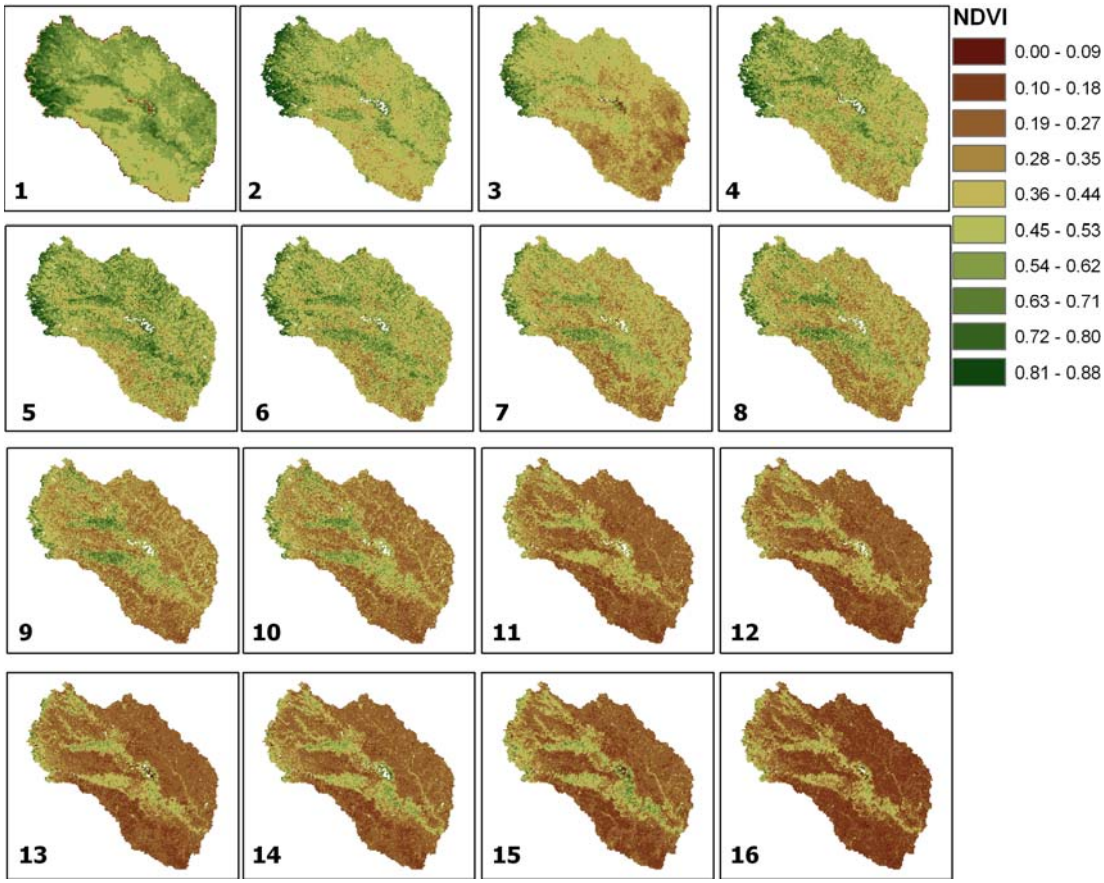

Figure 8: 16 MODIS NDVI image used in the land use classification

The 16 NDVI images were stacked into one image and an unsupervised classification using the K-means clustering was applied. Initially 15 clusters were chosen and a 0.95 convergence criterion was applied. The 15 classes were grouped into 7 major land use classes based on a field visit and a visual inspection using the Google Earth application[4], the old land use map and an additional decision rule using the slope derived from the SRTM DEM. The additional decision rule was required to distinguish between supplemental irrigated agriculture and low density forests and between irrigated agriculture and high density forests. Areas with slopes over 4% were classified as low density and high density forest respectively. The specifics of each class are shown in Table 2.

Class name	Cluster #	Slope criterion	Area (ha)	Area %
Water	1	N/A	38950	0.9
Rangelands	2-4	N/A	1228175	26.8
Rainfed agriculture	5-8	N/A	1536194	33.6
Supplemental irrigated agriculture	9-11	< 4% (11)	613575	13.4
Irrigated agriculture	12-15	< 4% (15)	910775	19.9
Forest high density	11	> 4%	143363	3.1
Forest low density	15	> 4%	103369	2.3

[4] http://earth.google.com

Table 2: Specifics of the land use classes

Rain fed agriculture covers the largest area in the basin (33.6%), but there are also considerable irrigated areas. The supplemental irrigated agriculture class covers around 13.4% of the basin area. These are areas which do not obtain their irrigation water from the large scale reservoirs but from groundwater or small tanks. The large command areas downstream of the major reservoirs cover a total area of 19.9%. The final LULC map is shown in Figure 9.

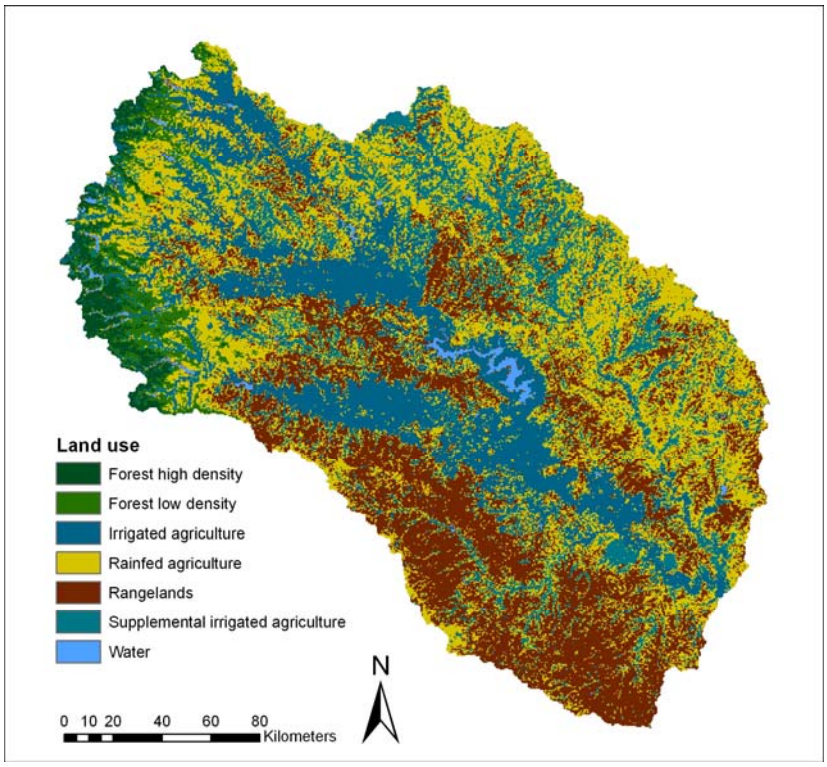

Figure 9: LULC map Upper Bhima

Table 3 shows a comparison between the acreages of each class in the old and the new classification. The differences are considerable. The area under rain fed agriculture has been reduced considerably (from 52.8% to 33.6%), while the area under irrigated agriculture has increased (4.4% to 19.9%). The forested areas in the Western Ghats are now also well depicted in the classification.

Class name	**Area % (old)**	**Area % (new)**
Water	0.7	0.9
Rangelands	29.6	26.8
Rainfed agriculture	52.8	33.6
Supplemental irrigated agriculture	11.9	13.4
Irrigated agriculture	4.4	19.9
Forest high density	0.5	3.1
Forest low density	0.0	2.3

Table 3: comparison between the two land use classifications

4 Evapotranspiration mapping

4.1 SEBAL

SEBAL provides a way to estimate and monitor actual ET with spatial sensitivity, without having to have soil moisture, land use and vegetation conditions. SEBAL solves the surface energy balance for heterogeneous terrain on the basis of reflected solar radiation and emitted thermal radiation (surface temperature). The actual ET (ETact) fluxes from SEBAL reflect the effects of various natural factors that influence ET, such as moisture availability, presence of pests and disease, salinity, and other factors. The standard ET equations are designed to compute potential ET, or the level of ET that would occur under optimal or "pristine", although sometimes general corrections are applied for conditions where water is limiting limitations by using a reduction coefficient (ETact=β ETpot, e.g. Budyko, 1969).

SEBAL is one of the first mathematical procedures that can operationally estimate spatially distributed ETact from field to river basin scale over an unlimited array of land use types, including desert soil, open water bodies, sparse natural vegetation, rainfed crops, irrigated crops, etc. The SEBAL model solves the energy balance for every every individual MODIS and Landsat pixel, thereby providing the spatial sensitivity. Satellite images need to be cloud-free to be processed for energy balance purposes.

The three primary bio-physical inputs from MODIS and Landsat images into SEBAL are (i) surface temperature, (ii) surface albedo and (iii) Normalized Difference Vegetation Index (NDVI) (see Figure 10). All of these parameters are measured directly or derived from measurements recorded by satellite-based sensors. In addition to that, a water mask is created. The water mask is meant for the assignment of particular values that are applicable to water only: emissivity, surface resistance, and soil heat flux/net radiation fraction. The latter fraction is relevant because the equations for soil heat flux for land and water are completely different. An existing generalized land use map is necessary to assign vegetation heights for the computation of the surface roughness for all pixels. This vegetation height is only considered for the turbulent parameters (i.e. momentum flux) and not for anything else. The inputs to SEBAL consists of (i) satellite multi-spectral radiances, (ii) routine weather data and (iii) DEM.

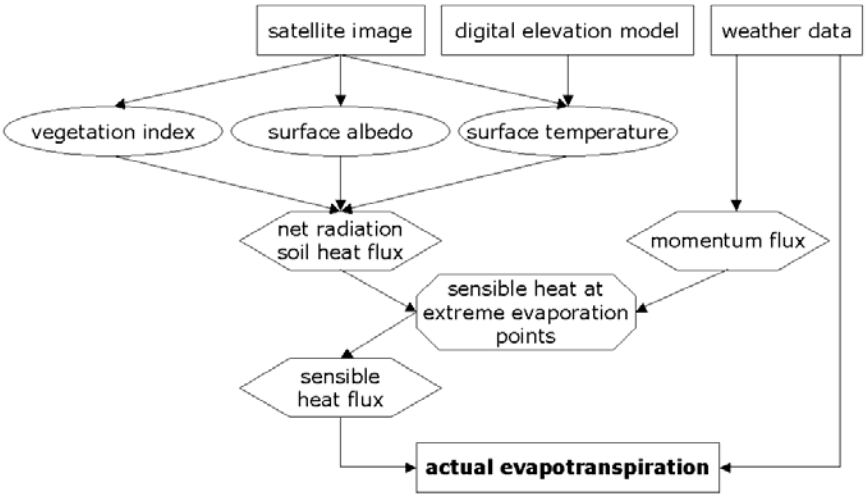

Figure 10: Data flow and key steps for the determination of spatially distributed ET fluxes according to the SEBAL method

SEBAL uses a set of algorithms to solve the energy balance at the earth's surface. The instantaneous ET flux is calculated for each pixel within a remotely sensed image as a 'residual' of the surface energy budget equation:

$$\lambda E = Rn - G - H \quad (1)$$

where λE is the latent heat flux (W/m2) (which can be equated to ET), Rn is the net radiation flux at the surface (W/m2), G is the soil heat flux (W/m2), and H is the sensible heat flux to the air (W/m2).

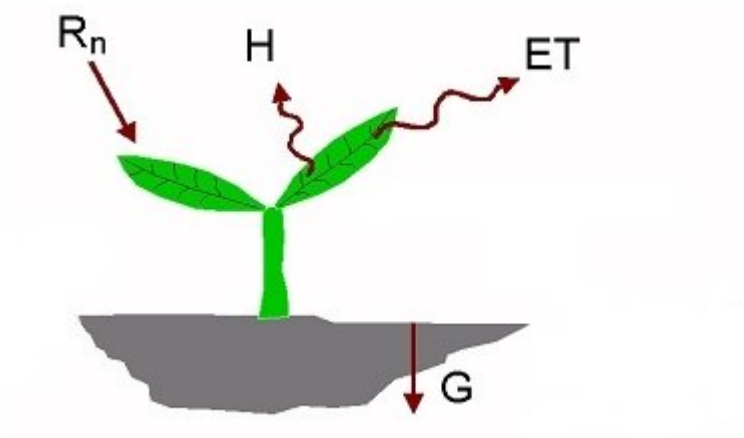

Figure 11: Main terms of the Surface Energy Balance

Rn represents the actual radiant energy available at the surface. It is computed by subtracting all outgoing radiant fluxes from all incoming radiant fluxes. This is further specified in the surface radiation balance equation:

$$Rn = RS\downarrow - \alpha\, RS\downarrow + RL\downarrow - RL\uparrow - (1 - \varepsilon 0)\, RL\downarrow \quad (2)$$

where $RS\downarrow$ is the incoming short-wave radiation (W/m2), α is the surface albedo (dimensionless), is the incoming long wave radiation (W/m2), $RL\uparrow$ is the outgoing long wave radiation (W/m2), and εo is the surface thermal emissivity (dimensionless).

In Eq. (2), the net short-wave radiation ($RS\downarrow - \alpha\, RS\downarrow$) that remains available at the surface is a function of the surface albedo (α). The broad band surface albedo α is derived from the narrow band spectral reflectances $\alpha(\lambda)$ measured by each satellite band. The incoming short-wave radiation ($RS\downarrow$) is computed using the solar constant, the solar incidence angle, a relative earth-sun distance, and a computed broad band atmospheric transmissivity. In this application of SEBAL, atmospheric transmissivity was obtained from a few selected automatic weather stations in Nevada that sustained the data integrity check. The incoming long wave radiation ($RL\downarrow$) was computed using a modified Stefan-Boltzmann equation with an apparent emissivity that is coupled to the shortwave atmospheric transmissivity and a measured air temperature. Outgoing long wave radiation (RL) is computed using the Stefan-Boltzmann equation with a calculated surface emissivity and surface temperature. Surface temperature is derived from the narrow-band satellite measurements of thermal infrared radiation.

The challenge in energy balance modeling is to partition net radiation into sensible (H) and latent heat fluxes (λE). To guide this partitioning process, extreme values of H are defined for 'hot' and 'cold' pixels selected by the operator. The hot pixel has a high surface temperature associated with the absence of evaporative cooling. Characteristics that qualify pixels for consideration as "hot" pixels are as follows: (i) their surface temperatures occur near the upper end of the frequency distribution of all pixels in the image, (ii) they have relatively sparce vegetative cover (as indicated by NDVI) and (iii) they appear to consist of essentially bare land on the false color composite.

In contrast, characteristics that qualify pixels for consideration as "cold" pixels are as follows: (i) their surface temperatures occur near the lower end of the frequency distribution, (ii) they appear to be within open water surfaces or well irrigated fields and (iii) they have a low reflectance in the visible part of the spectrum. For each image processed, the operator must decide which pixels to select as the hot and cold pixels.

At the hot pixel it is assumed that ET is zero; thus, $H \approx Rn-G$. At the cold pixel, it is assumed that sensible heat is very small or zero, because all or most of the net available energy is used for ET; thus, $\lambda E \approx Rn-G$. The sensible heat does not necessarily have to be exactly zero, but it should be small.

Select of the hot and cold pixels for each image constrains the range of sensible heat within realistic bounds, essentially providing a self-calibrating feature, with the H fluxes for all other pixels lying between. Interpolation between these two bounds is done according to a linear function of surface temperature where the a and b coefficients are obtained from linking H to the surface temperature at the hot and cold pixels:

$$H = \{\rho a\ cp\ u^*\ (a + b\ T0)\} / \{\ln(z2/z1) - \psi h\ (z2,L) + \psi h\ (z1,L)\} \quad (3)$$

Where ρa (kg/m3) is the moist air density, cp (J/kg/K) is the specific heat at constant pressure, u* (m/s) is the friction velocity, z (m) is the near-surface reference height to which the a,b coefficients as well as the constant H flux applies, ψh (-) is the stability correction for heat transport and L (m) is the Monin Obukhov length. Eq. (3) requires single layer wind speed observations and surface roughness for the determination of friction velocity u* to be known:

$$u^* = \{u(z2)\ k\} / \{\ln(z2/z0m) - \psi m\ (z2,L) + \psi m\ (zom,L)\} \quad (4)$$

where z0m (m) is the surface roughness length for momentum transport and k (-) the von Karman's constant. SEBAL uses an iterative process to correct for atmospheric instability caused by buoyancy effects of surface heating. The surface roughness z0m is computed from estimates of vegetation height based on a simple land use mask and the actual LAI following the simple roughness model of Raupach (1994) and suggestions of model performance tests published by Verhoef et al. (1997).

In Eq. (1), the soil heat flux (G) and sensible heat flux (H) are subtracted from the net radiation flux at the surface (Rn) to compute the "residual" energy available for evapotranspiration (λE). Soil heat flux is empirically calculated as a G/Rn fraction using instantaneous surface temperature and an approximation for near-surface soil temperature at sunrise. A light interception reduction function is applied for the presence of foliage using NDVI as an indicator for canopies.

The λE time integration in SEBAL is split into two steps. The first step is to convert the instantaneous latent heat flux (λE) into daily λE24 values by holding the evaporative fraction constant. The evaporative fraction EF is:

$$EF = \lambda E / (Rn - G) \quad (-) \quad (5)$$

Field measurements under various environmental conditions indicate that EF is nearly constant with time during the diurnal cycle. Thus, because EF ~ EF24, the 24 hour latent heat flux can be approximated by:

$$\lambda E24 = EF\ \xi\ (Rn24 - G24) \quad (W/m2) \quad (6)$$

where ζ (-) is an advection enhancement parameter. It is assumed that the evaporative fraction EF specified in Eq. (5) remains quasi-constant during daytime hours and that variations can be related to advection ξ. Experimental work has demonstrated that this holds true for environmental conditions where soil moisture does not significantly change (e.g. Shuttleworth et al., 1989; Brutsaert and Sugita, 1992; Nicols and Cuenca, 1993; Kustas et al., 1994; Crago, 1996; Farah, 2001). This needs to be true for single days only to get an appropriate value for λE24 during satellite overpass days.

Advection occurs when hot desert air is blown over irrigated areas, typically in the afternoon, by winds driven by differences in air densities. The regional scale atmospheric circulation adds extra energy to moist vegetation. This extra energy can increase ET to the extent that it exceeds the net available energy (Rn-G0), which from an energy balance point of view implies that the sensible heat flux is directed towards the surface (H is negative).

Within SEBAL, advection is incorporated into the ζ parameter that varies with the weather conditions and the moisture of the underlying soils. The impact of weather conditions on advection is expressed by the changes of the evaporative fraction of the reference crop EFgrass between satellite overpass and the 24-h counterpart governed by day and night weather conditions. The influence of advection decreases non-linearly with soil moisture content, which implies that only wet surface are exposed to advection.

Depending on the time scale chosen, different time integrations of (Rn- G0) need to be obtained. For the daily time scale, ET24 is formulated as:

$$ET_{24} = \frac{86400 \cdot 10^3}{\lambda \rho_w} \lambda E24 \qquad \text{(mm d-1)} \qquad (7)$$

where Rn24 (W m-2) is the 24-h averaged net radiation, λ (J kg-1) is the latent heat of vaporization, ρw (kg m-3) is the density of water.

The second step is the conversion from a daily latent heat flux into 14-day values, which was achieved by application of the Penman-Monteith equation:

$$\lambda E24PM = (sa\ Rn24 + \rho acp\ \Delta e/ra) / (sa + \gamma\ (1 + rs/ra)) \qquad (W/m2) \qquad (8)$$

where sa (mbar/K) is the slope of the saturated vapor pressure curve, ρacp (J/m3 K) is the air heat capacity, Δe (mbar) is the vapor pressure deficit, γ (mbar/K) is the psychrometric constant and ra (s/m) is the aerodynamic resistance. The parameters sa, Δe and ra are controlled by meteorological conditions, and Rn and rs by the hydrological conditions.

The SEBAL computations can only be executed for cloudless days. The result of λE24 from Eq. (6) has been explored to convert the Penman-Monteith equation (8) and to quantity rs inversely using λE24= λEPM. The spatial distribution of rs so achieved, will consequently be used to compute λE24 by means of Eq. (8) for all days without satellite image available (e.g. Farah, 2001). The total ETact for a given period can be derived from the shorter term average values of sa, Δe, ra and Rn

The standard 250 m Digital Elevation Model (DEM) has been used for the correction of air pressure and related air density and psychrometric constant at higher elevation. The DEM is also used to correct the absorbed solar radiation values, both for slope and aspect. Southern facing terrain due to the angle of incidence absorb, namely, more solar radiation per unit land than the Northern facing slope.

4.2 Reference evapotranspiration

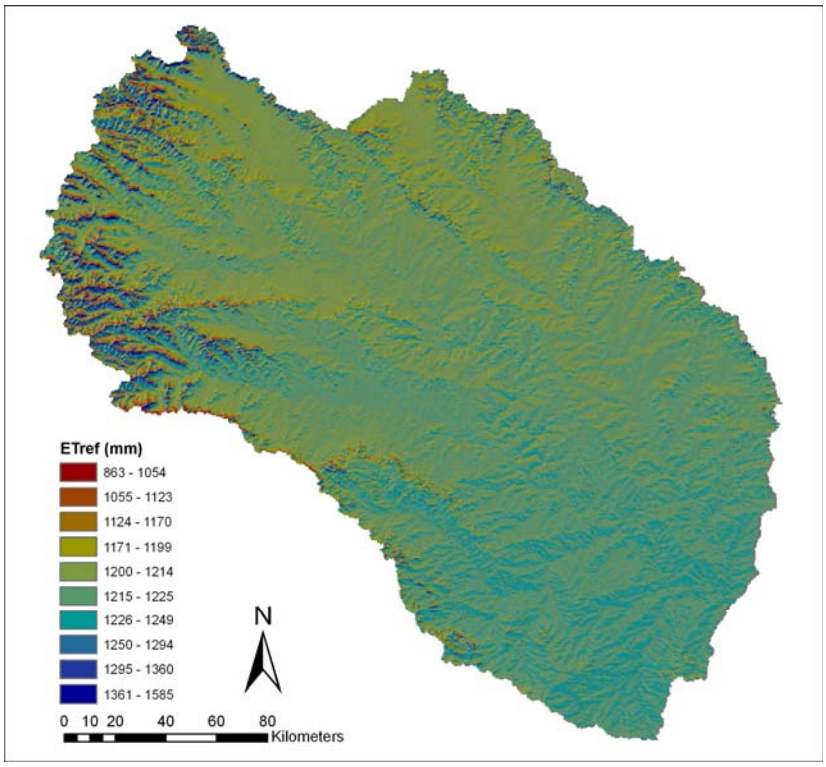

Figure 12: Total reference evapotranspiration from 1 October 2004 to 31 May 2005

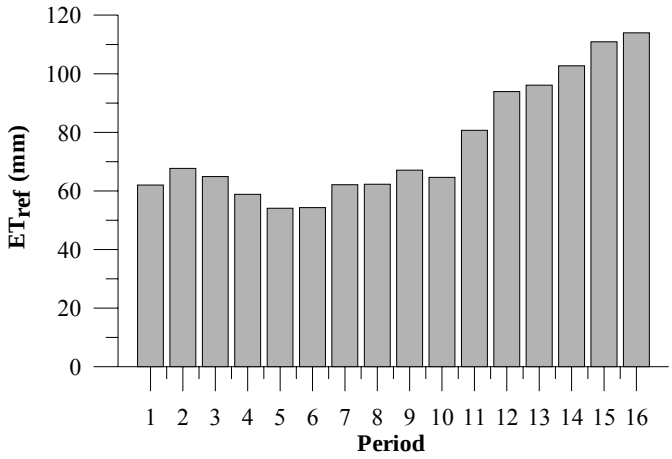

Figure 13: Bi-weekly reference evapotranspiration from 1 October 2004 to 31 May 2005

4.3 Potential Evapotranspiration

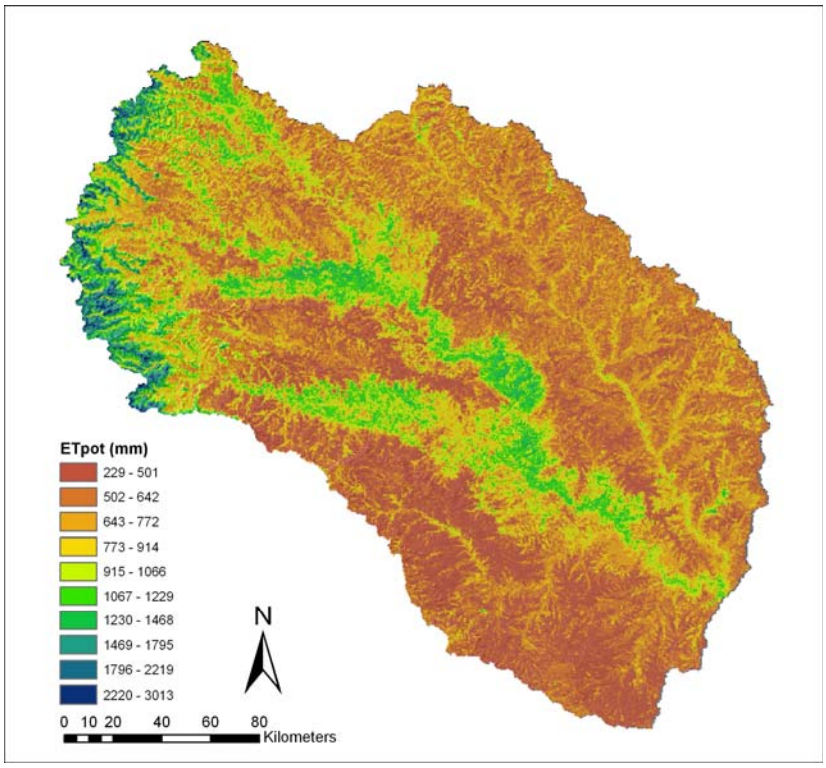

Figure 14: Total potential evapotranspiration from 1 October 2004 to 31 May 2005

4.4 Actual Evapotranspiration

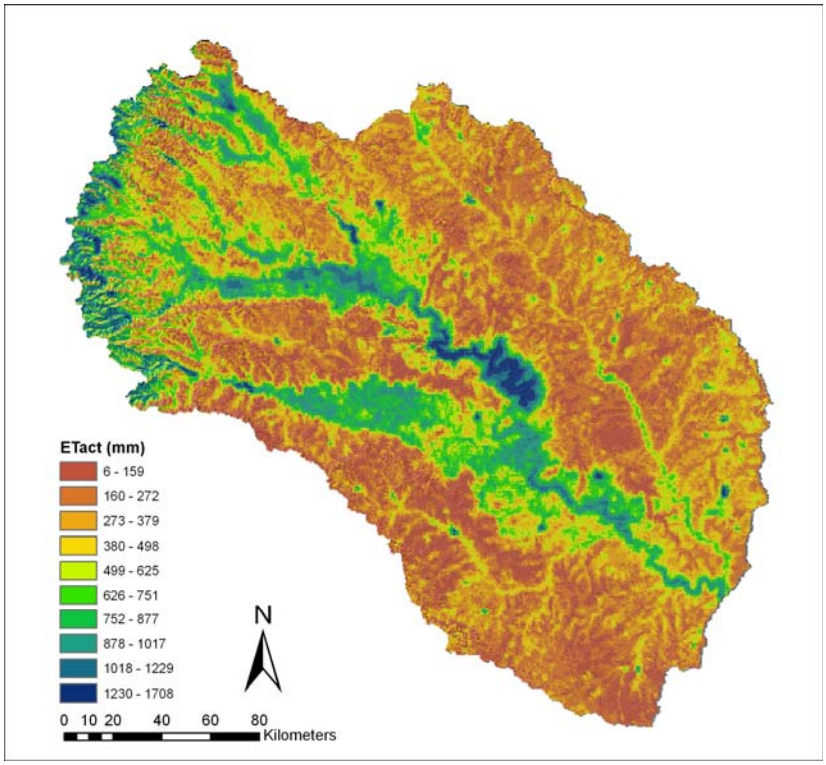

Figure 15: Total actual evapotranspiration from 1 October 2004 to 31 May 2005

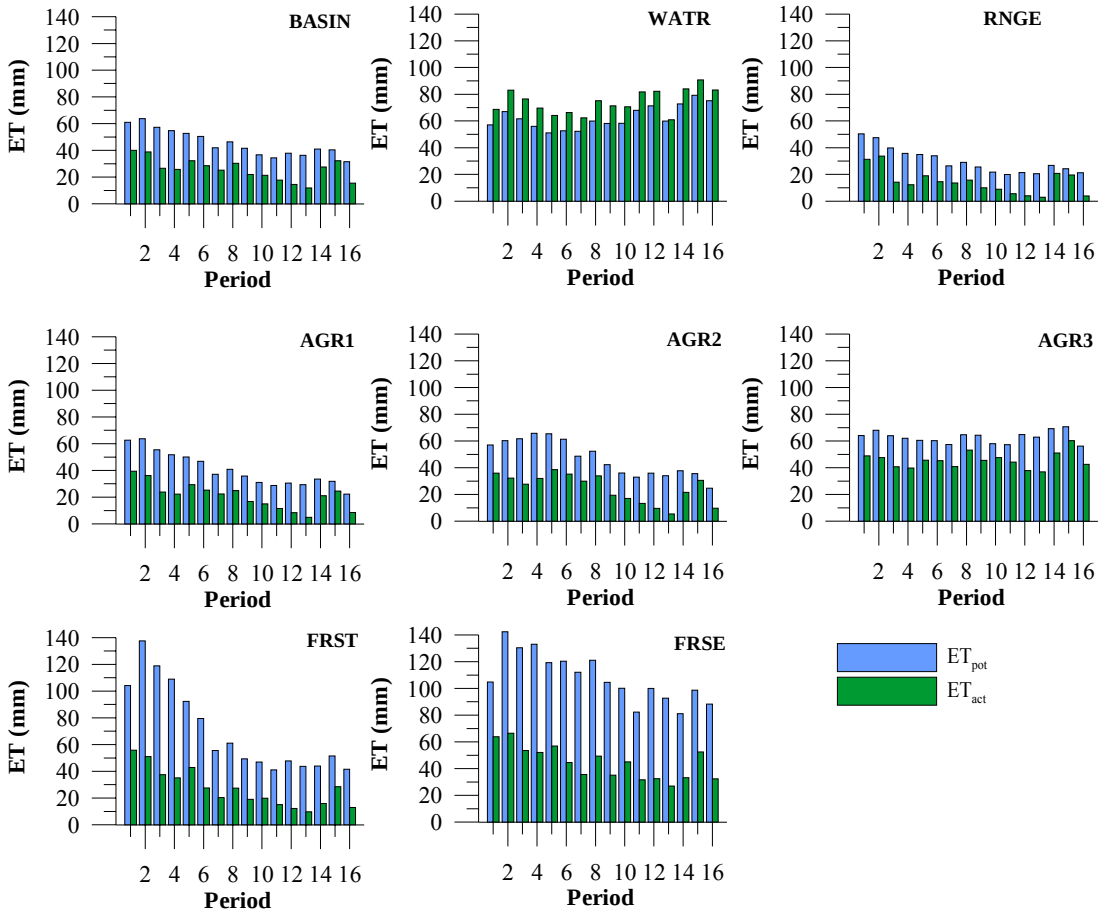

Figure 16: Bi-weekly potential and actual evapotranspiration per land use from 1 October 2004 to 31 May 2005

4.5 Biomass production

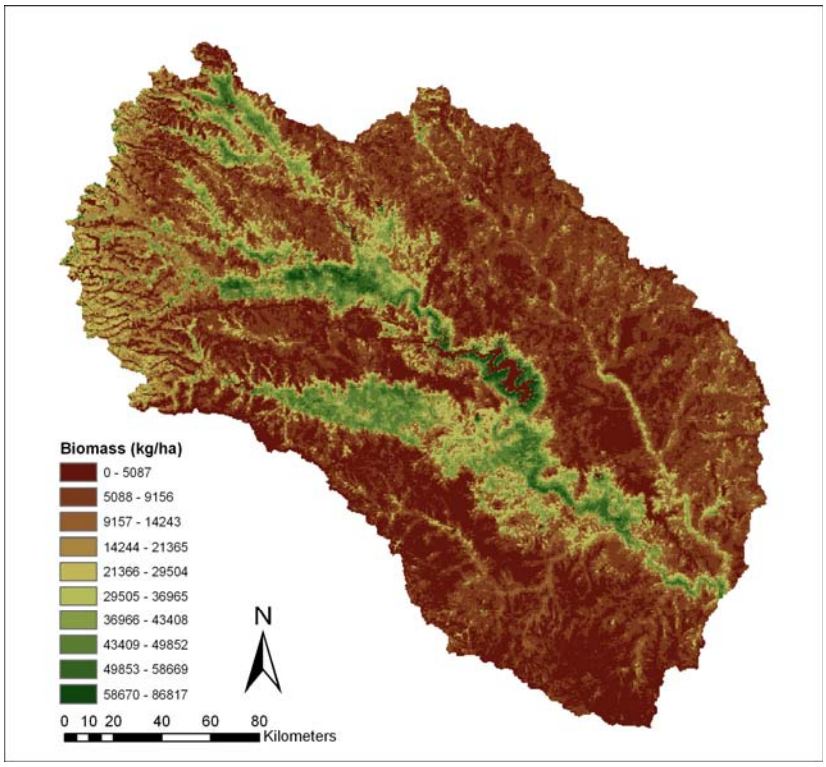

Figure 17: Total biomass production from 1 October 2004 to 31 May 2005

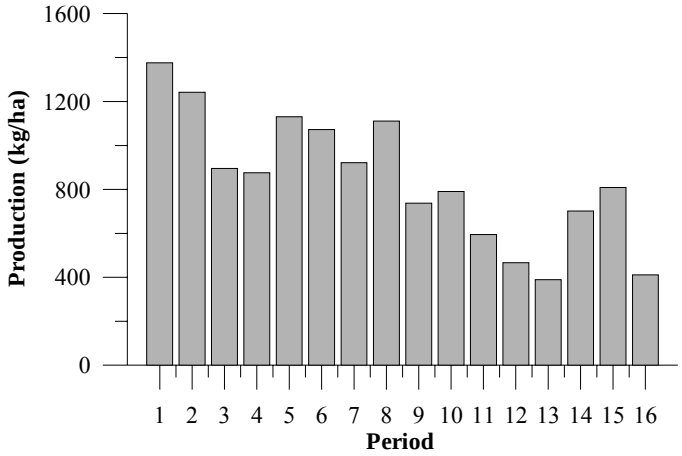

Figure 18: Bi-weekly biomass production from 1 October 2004 to 31 May 2005

5 Precipitation mapping using Remote Sensing

5.1 Introduction

A limited set of precipitation data from meteorological stations is available for the Upper Bhima catchment. A dataset with monthly precipitation data for eight Indian Meteorological Department (IMD) stations and for 15 additional stations from the National Data Centre (NDC) in Pune were available. The location, source and time coverage of the data is shown in Figure 19.

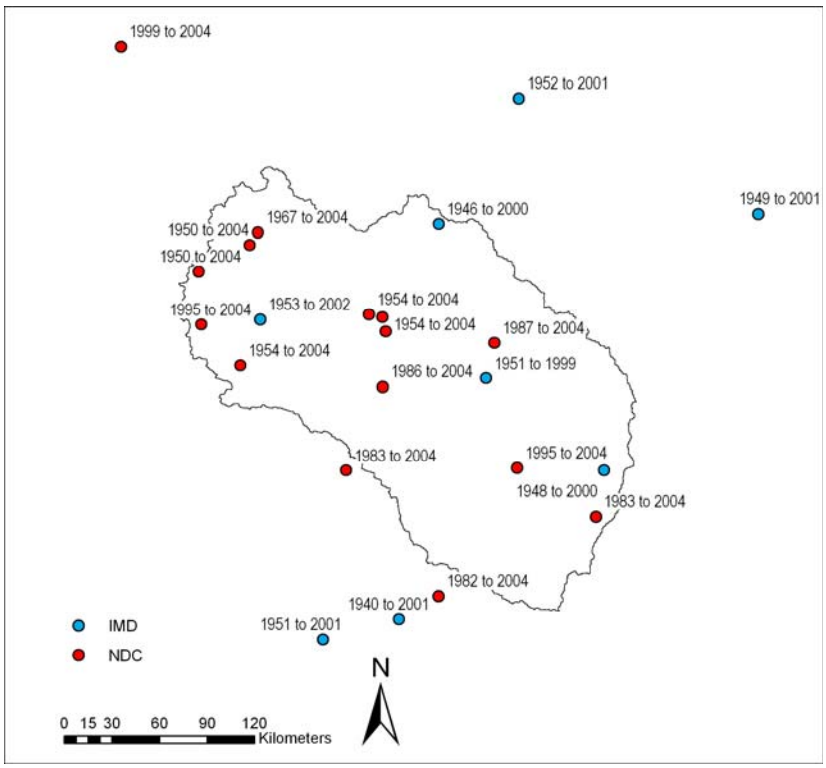

Figure 19: Location, source and time overage monthly precipitation data

Since there is an extreme spatial variation in precipitation ranging from 2000 mm in the Western Ghats to 650 mm in the most eastern part of the sub-basin it is important to have a dense network of meteorological stations. In this study SEBAL evapotranspiration maps will be used to calibrate the hydrological model. SEBAL data are available from October 2004 until May 2005, but precipitation data are only available up to 2004 for a limited number of stations. For these reasons Remote Sensing derived precipitation from the Tropical Rainfall Monitoring Mission (TRMM) is used in this study.

5.2 *Tropical Rainfall Monitoring Mission*[5]

The Tropical Rainfall Measuring Mission (TRMM) is a joint space project between NASA and the Japanese Aerospace Exploration Agency (JAXA). TRMM is designed to measure tropical precipitation and its variation from a low-inclination orbit combining a suite of sensors to overcome many of the limitations of remote sensors previously used for such measurements from space. The fundamental objective of TRMM is to understand the role of latent heat in driving the circulation of the global atmosphere. With the inclusion of rain radar, TRMM will provide the first opportunity to estimate the vertical profile of the latent heat that is released through condensation. The TRMM rainfall data is particularly important for studies of the global hydrological cycle and for testing the realism of climate models, and their ability to simulate and predict climate accurately on the seasonal time scale. Other scientific issues such as the effects of El Niño on climate could be addressed with a reliable, extended time series of tropical rainfall observations as well. The TRMM satellite has a latitudinal range from 50°S - 50 °N. The TRMM satellite has been launched November 27 in 1997 and the mission has recently been extended to 2009.

The observatory for rainfall observations consists of a precipitation radar, a multi-frequency microwave radiometer and a visible and infrared (VIS/IR) radiometer. Used in this combination in a complementary way, these sensors, with the designed orbit of 350 km altitude and inclination of 35°, will meet the measurement accuracy for rainfall needed to fulfill the stated science objectives of the mission. For related precipitation observations (i.e., lightning) and for additional important climate observations, a lightning imager and an Earth radiation budget sensor have been added. A brief description of each of the five instruments is included here:

- The Precipitation Radar (PR), the first in space, will measure the 3-D rainfall distribution over both land and ocean. More specifically, this instrument will define the layer depth of the precipitation and provide information about the rainfall reaching the surface, the key to determining the latent heat input to the atmosphere. A unique feature is that it will permit the measurement of rain over land where passive microwave channels have more difficulty. The PR is an electronically scanning radar operating at 13.8 GHz with horizontal polarization using a 128-slotted waveguide antenna and solid state power amplifiers to develop an active phased array. The horizontal resolution is 4.3 km at nadir, the range resolution is 250 m and the scanning swath width is 220 km.
- The multi-channel microwave radiometer, designated as the TRMM Microwave Imager (TMI), is designed to provide information on the integrated column precipitation content, its areal distribution, and its intensity. The horizontal resolution will allow the definition and investigation of most rainfall types, including convective cells. The technique is best suited for estimates over oceans, where data are needed most for climate model verification. The TMI will operate on 5 frequencies, of which 4 will have dual polarization thus providing 9 channels of data. The 5 frequencies are 10.65 GHz, 19.35 GHz, 22.235 GHz (single polarization), 37.0 GHz and 85.5 GHz. The horizontal resolution of the TMI will range from 5 km at 85.5 GHz to 45 km at 10.65 GHz. A scan angle of 65° will provide a swath width of 760 km.
- The Visible Infrared Scanner (VIRS) will provide very high resolution information on cloud coverage, type, and cloud top temperatures and also serve as the link between these data

[5] http://trmm.gsfc.nasa.gov/

and the long and virtually continuous coverage by the geosynchronous meteorological satellites. The VIRS is a 5 channel cross-track scanning radiometer operating at 0.63, 1.6, 3.75, 10.80, and 12.0 microns. The instrument, with a swath width of 720 km, will provide cloud distributions by type and height and rain estimates from brightness temperatures at a horizontal resolution of 2.1 km (nadir). Direct correlation with PR and TMI measurements will assist in providing more accurate rain estimates from VIRS thereby enhancing its capability for verifying or calibrating the rain estimates from operational meteorological satellites.

- The Lightning Imaging Sensor (LIS) is designed to investigate the global incidence of lightning, its relationship with the global electric circuit, and, in conjunction with the PR, TMI, and VIRS, its correlation with rainfall. Lightning is not a necessary condition for tropical rainfall such as warm rain or even for some convective rainfall in the tropics. However, when updrafts and downdrafts are sufficient to cause lightning, rainfall results. LIS will be optimized to detect the lightning location, mark the time of occurrence, and measure the radiant energy. LIS is a calibrated optical sensor operating at 0.7774 microns and will observe the distribution and variability of lightning over the Earth. The horizontal resolution at nadir will be 5 km and the swath width will be 590 km.

Several orbital and gridded data products are available for download at the Goddard Distributed Active Archice Centre (DAAC)[6]. For this study the 3B-43 product is used. The global rainfall algorithm (3B-43) combines the estimates generated by combined instrument rain calibration (3B-42) and global gridded rain gauge data from CAMS, produced by NOAA's Climate Prediction Center and/or global rain gauge product, produced by the Global Precipitation Climatology Center (GPCC). The output is rainfall for 0.25x0.25 degree grid boxes for each month.

5.3 *Downscaling and calibration of TRMM data*

For the model simulation the irrigation year June 2004 to May 2005 will be used in the simulations. SEBAL data are available from October 2004 to May 2005.

The total precipitation at the original resolution from June 2004 to May 2005 is shown on the left side of Figure 22. The 0.25 degree resolution is still too coarse for application in a simulation model. Therefore a downscaling procedure is developed and applied to the data. For all meteorological stations in the sub-basin which cover the period 1998-2004 the monthly TRMM data were extracted. For each station a regression analysis was performed on the monthly precipitation amounts.

[6] http://disc.sci.gsfc.nasa.gov/data/datapool/TRMM/01_Data_Products/index.html

Station	Slope	Intercept	R^2
Ambavade-2	0.26	21.94	0.29
Askheda	0.80	18.15	0.80
Barur (Takali)	0.59	16.34	0.51
Chaskman	1.06	11.79	0.81
Kashti	0.40	18.49	0.37
Khamgaon	0.86	18.29	0.65
Late	0.47	2.65	0.50
Pargaon	0.84	20.15	0.64
Rosa (Kolgaon)	0.71	15.34	0.57
Sakhar	1.09	0.84	0.82
Shirur	0.32	12.69	0.45
Sidhewadi	0.58	19.03	0.51
Wegre (Muthe)	0.70	37.58	0.68

Table 4: Slope, intercepts and R^2 for the 13 selected meteorological stations

Table 4 shows the slopes, intercepts and R^2 values of the regression analysis. The R^2 values vary from 0.29 (Ambavade-2) and 0.82. For Askheda and Sakhar the scatter plots are shown in Figure 20.

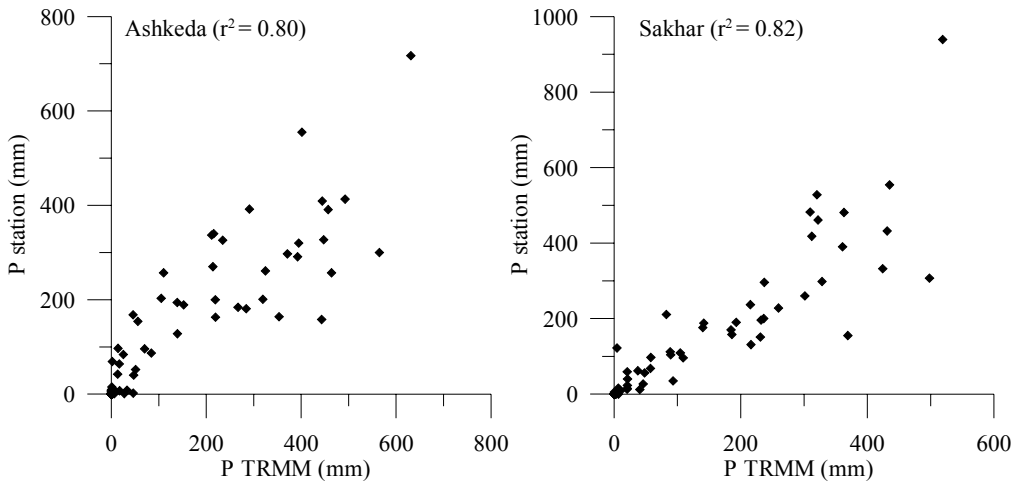

Figure 20: Scatterplots for monthly TRMM precipitation and observed precipitation from 1998-2004 for two meteorological stations

The next step in the downscaling procedure is the spatial interpolation of the slopes and intercepts of the meteorological stations (Figure 21). To avoid erroneous precipitation amounts, especially in the dry seasons, only those station with an $R^2 > 0.50$ and an intercept < 20 are used in the interpolation (7 stations). The slopes range from 0.57-1.10 and the intercepts range from 0-22 mm/month.

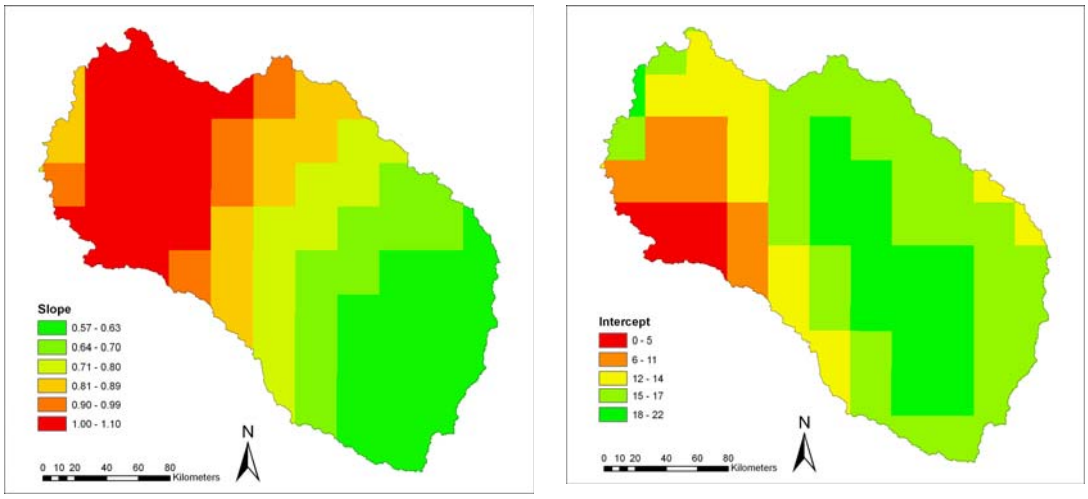

Figure 21: Slope and intercept used to scale TRMM derived precipitation

The final step in the procedure is to convert the centers of the TRMM grid boxes to points and to interpolated these points to a raster of a higher resolution (0.005 degrees by 0.005 degrees). A spline tension interpolator was used with weight 1 and using 4 surrounding points (Franke, 1982). The result of this downscaling procedure is shown in Figure 22.

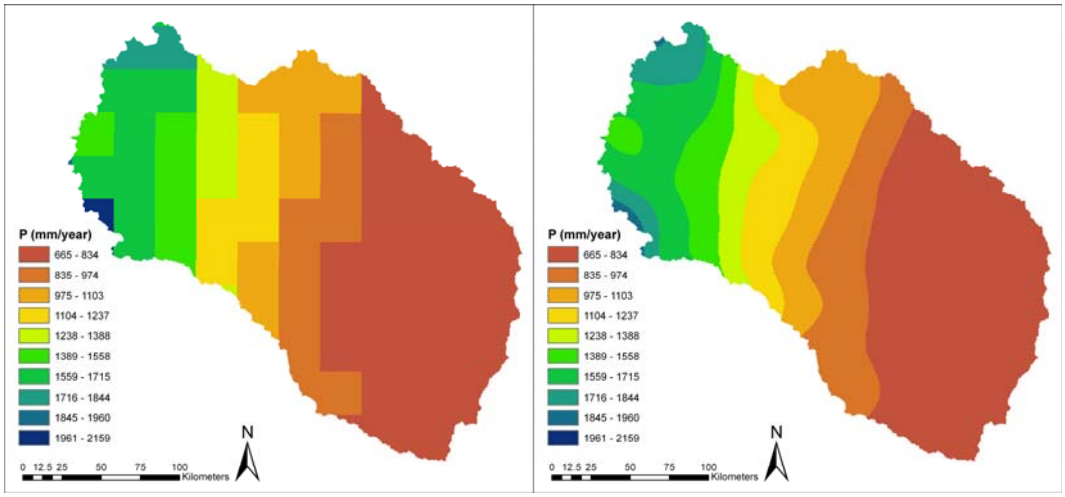

Figure 22: Total precipitation from June 2004 to May 2005. The scaled TRMM data is shown in the left figure and the downscaled TRMM data is shown in the right figure.

This downscaling procedure is repeated for each month between June 2004 and May 2005. Figure 23 shows the monthly precipitation in the basin. Precipitation is clearly concentrated in the monsoon months from June to September with the peak in July 2005. There is a clear decreasing trend from the western to the eastern part of the sub basin.

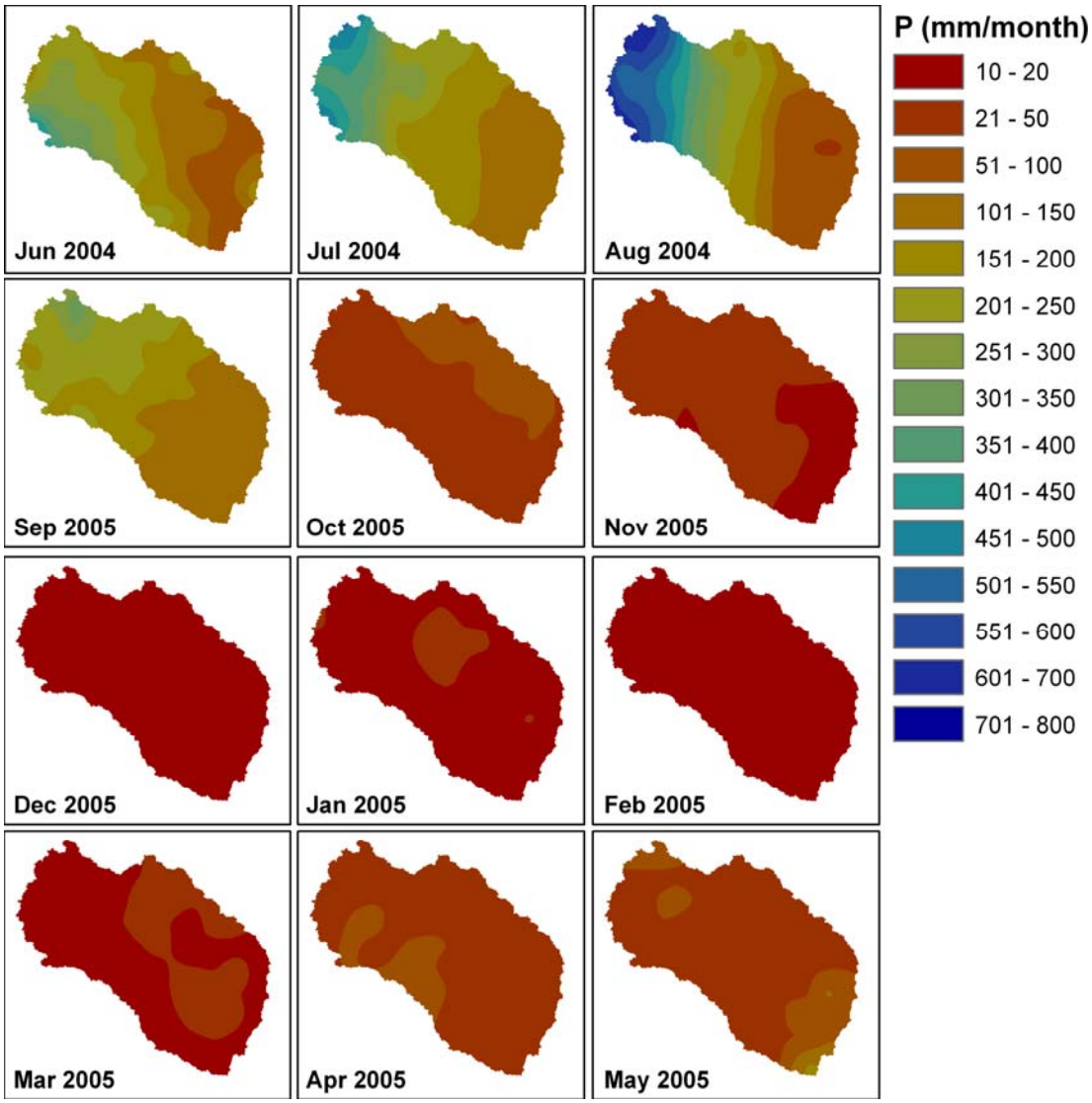

Figure 23: Monthly downscaled TRMM derived precipitation in the Upper Bhima sub basin

6 Modeling the Upper Bhima catchment

The SWAT model of the Upper Bhima catchment is created in several consecutive steps, which are described in this chapter. Based on the topography the catchment is subdivided into smaller units (sub- basins)

6.1 *Topography*

A Remote Sensing derived digital elevation model (DEM) acquired with Shuttle Radar Topographic Mission (SRTM)[7] is used to partition the catchments in sub-basins and rivers. GIS based hydrological surface function are used in an automated procedure of the SWAT GIS interface (AVSWAT). The original DEM has a spatial resolution of 90m, but to reduce calculation times the DEM is resampled to a spatial resolution of 250 m.

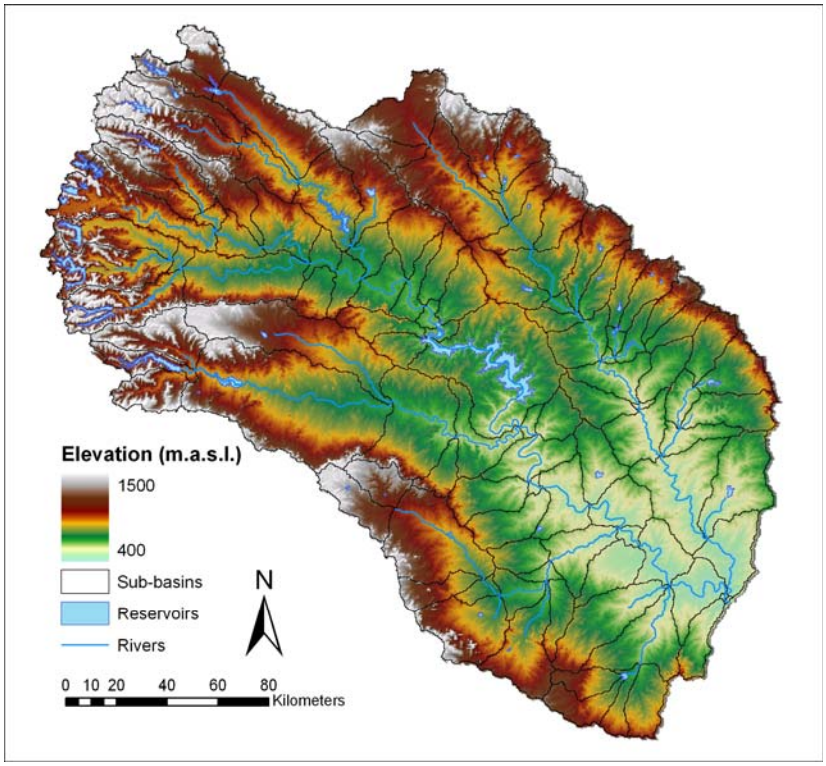

Figure 24: Digital elevation model, sub-basins, and major rivers

Figure 24 show the DEM of the catchment. The elevation ranges from 414m in the east of the catchment to 1458m in the western Ghats. The elevation distribution of the entire catchment is shown in Figure 25. It shows that nearly 95% of the area of the catchment is below 800m.

[7] http://www2.jpl.nasa.gov/srtm/

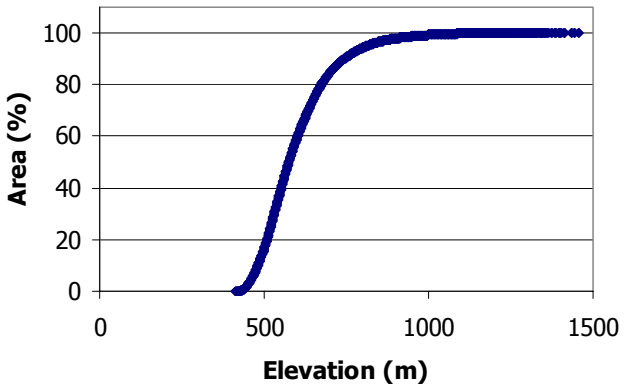

Figure 25: Elevation distribution in the catchment

The catchment has an area of 4.567.781 ha and a total of 115 sub-basins are delineated with a minimum area of 20.000 ha (Figure 24).

6.2 Soils

The FAO UNESCO digital soil map of the world is used in this study (FAO, 1995). The Digital Soil Map of the World (DSMW) CD-ROM is based on the FAO/UNESCO Soil Map of the World. The FAO-Unesco Soil Map of the World was published between 1974 and 1978 at 1:5.000.000 scale. The soil map of the world was prepared on the base of the topographic map series of the American Geographical Society of New York . The legend of the original soil map of the World (FAO, 1974) comprises an estimated 4930 different map units, which consist of soil units or associations of soil units. When a map unit is not homogeneous, it is composed of a dominant soil and component soils. The latter are: associated soils, covering at least 20 % of the area; and inclusions, important soils which cover less than 20 % of the area. The legend of the soil map of the world (1974) comprises 106 soil units (from Af to Zt), grouped in 26 major soil groupings. The soil map for the upper Bhima catchment is shown in Figure 26.

The majority of the alluvial plains in the catchment consist of chromic vertisols. Vertisols are churning heavy clay soils with a high proportion of swelling 2:1 lattice clays. These soils form deep wide cracks from the surface downward when they dry out, which happens in most years. Dry Vertisols have a very hard consistence; wet Vertisols are (very) plastic and sticky. It is generally true that Vertisols are friable only over a narrow moisture range but their physical properties are greatly influenced by soluble salts and/or adsorbed sodium. Infiltration of water in dry (cracked) Vertisols with surface mulch or a fine tilth is initially rapid. However, once the surface soil is thoroughly wetted and cracks have closed, the rate of water infiltration becomes almost zero. (The very process of well/shrink implies that pores are discontinuous and non-permanent.) If, at this stage, the rains continue (or irrigation is prolonged), Vertisols flood readily. The highest infiltration rates are measured on Vertisols that have a considerable shrink/swell capacity, but maintain a relatively fine class of structure. Not only the cracks transmit water from the (first) rains but also the open spaces between slickensided ped surfaces that developed as the peds shrunk. Data on the water holding capacity of Vertisols vary widely, which may be

attributed to the complex pore space dynamics. Water is adsobed at the clay surfaces and retained between crystal lattice layers. By and large, Vertisols are soils with good water holding properties. However, a large proportion of all water in Vertisols, and notably the water held between the basic crystal units, is not available to plants. Investigations in the Sudan Gezira have shown that the soil moisture content midway between large cracks changes very little, if at all, when the clay plain is flooded for several days or even several weeks. The soil's moisture content decreases gradually from more than 50 percent in the upper 20 cm layer to 30 percent at 50 cm depth. Deeper than 100 cm, the soil moisture content remains almost invariant throughout the year.

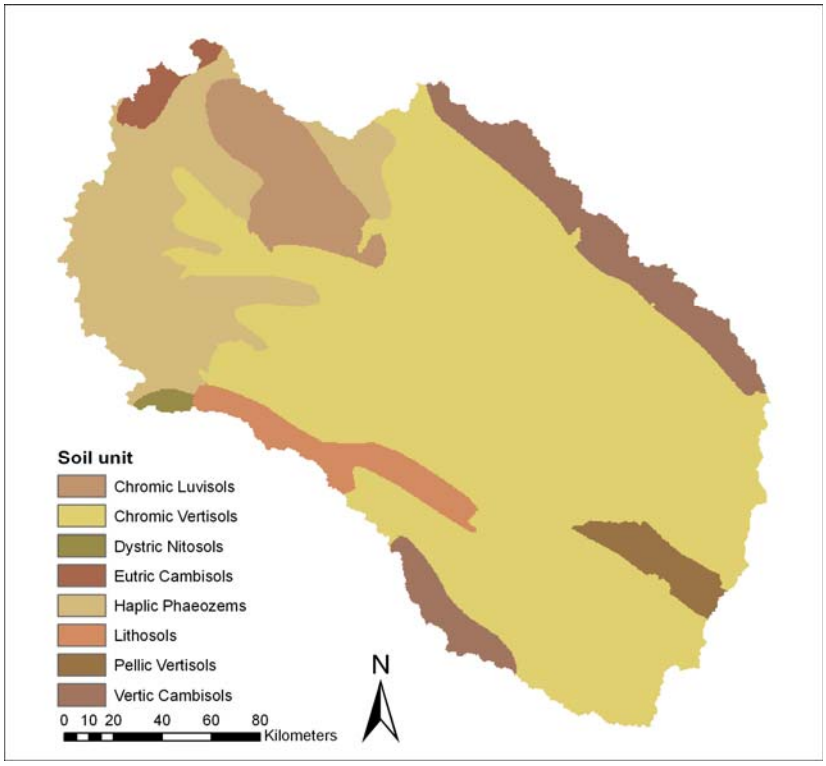

Figure 26: FAO/UNESCO soil map of the Upper Bhima catchment

The upland areas mainly have a luvisol soil type. This soil type is common in upland areas with a distinct wet and dry season. Luvisols have favourable physical properties; they have granular or crumb surface soils that are porous and well aerated. The `available' moisture storage capacity is highest in the argic horizon (15 to 20 volume percent). The argic horizon has a stable blocky structure but surface soils with a high silt content may be sensitive to slaking and erosion. Most Luvisols are well drained but Luvisols in depression areas with shallow groundwater may develop gleyic soil properties in and below the argic horizon. Stagnic properties are found where a dense illuviation horizon obstructs downward percolation and the surface soil becomes saturated with water for extended periods of time.

The physical properties needed for the SWAT model are also derived from the FAO soil map of the world. These are summarized in Table 5.

Table 5: Soil physical properties

Code	Description	Depth	AWC	Clay	Silt	Sand	Bulk density	Organic carbon content
		cm	mm/mm	%	%	%	g/cm3	%
Be66-2c	Eutric Cambisols	1280	0.21	22	35	43	1.21	0.79
Bv12-3b	Vertic Cambisols	1430	0.10	50	21	30	1.59	0.77
Hh11-2bc	Haplic Phaeozems	1368	0.15	28	24	48	1.51	0.52
I-Hh	Lithosols	950	0.17	21	21	58	1.45	0.56
Lc75-1b	Chromic Luvisols	1430	0.14	29	21	50	1.53	0.60
Nd51-2b	Dystric Nitosols	2250	0.19	34	18	48	1.19	0.74
Vc43-3ab	Chromic Vertisols	2150	0.20	32	16	52	1.20	0.52
Vc44-3a	Chromic Vertisols	1430	0.07	54	23	23	1.70	0.59
Vc45-3a	Chromic Vertisols	1550	0.07	58	19	23	1.71	0.41
Vp42-3a	Pellic Vertisols	1550	0.08	57	23	21	1.65	0.51

6.3 Hydrological Response Units

Hydrological Response Units (HRUs) are the smallest unit of calculation in the SWAT model and are defined as unique combinations of soil and land use. Before determining the HRUs a preprocessing step is taken. However an area threshold is specified for both soils and land use. This threshold determines whether a certain soil or land use class is used as an HRU based on the proportion of the total sub basin area the soil class or land use type has. The thresholds used are 10% and 5 % for soil and land use respectively. The HRUs are created using an automated procedure in the AVSWAT interface. A total of 768 HRU are generated. A map with the HRUs is shown in Figure 27.

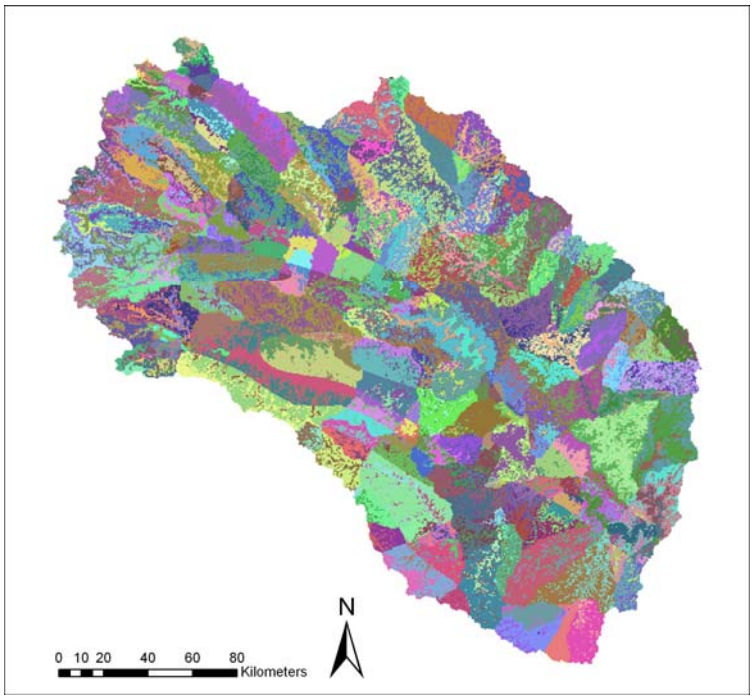

Figure 27: Hydrological Response Units in the catchment

6.4 *Meteorology*

The SWAT model requires the following daily meteorological parameters:

- Solar radiation
- Minimum and maximum temperature
- Relative humidity
- Wind speed
- Precipitation

Different sources of information have been used to derive the daily weather data from 1 June 2004 to 31 May 2005. For all parameters data are used for two different meteorological stations; one in Pune and one in Sholapur (Figure 28). Similar to the procedure in SEBAL: the data of the two stations have been averaged. For precipitation a virtual meteorological station is created for each of the 112 subbasins.

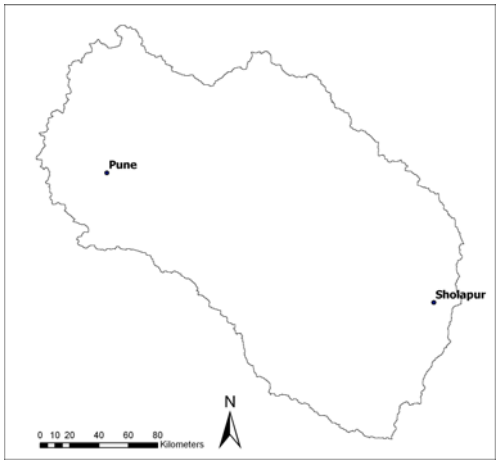

Figure 28: Location of the meteorological stations

6.4.1 Solar radiation

The solar radiation is defined as the amount of radiation reaching a horizontal plan on the earth's surface. First the extraterrestrial radiation at the top of the atmosphere was calculated, which is then corrected for scattering, reflection and adsorption by atmospheric gases, clouds and dust. The extraterrestrial radiation is depending on the latitude and the Julian day in the year. The amount of solar radiation (Q_s (MJ m^{-2} day^{-1})) reaching the surface of the earth is calculated using the Angström formula:

$$Q_s = \left(a_s + b_s \frac{n}{N} \right) \cdot Q_a$$

Where a_s(-) is a regression constant, expressing the fraction of extraterrestrial radiation reaching the earth on overcast days, a_s+b_s is the fraction of extraterrestrial radiation reaching the earths surface on

clear days, n/N (-) is the relative sunshine duration and Q_a (MJ m^{-2} day^{-1}) is the extraterrestrial radiation. Values of 0.25 and 0.50 are used for a_s and b_s respectively.

Solar radiation is calculated for both Pune and Sholapur (Figure 29). The relative sunshine duration is derived from the IWMI climate atlas[8].

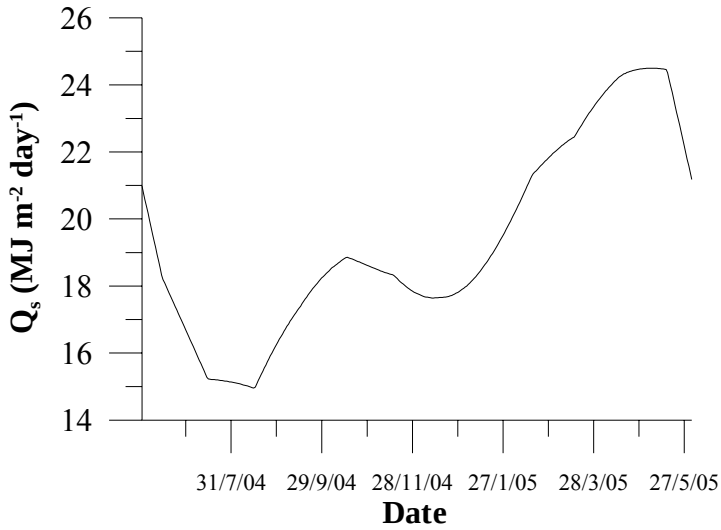

Figure 29: Average daily solar radiation Pune and Sholapur

6.4.2 Temperature

Public domain data[9] are used for daily maximum and minimum temperature (Figure 30).

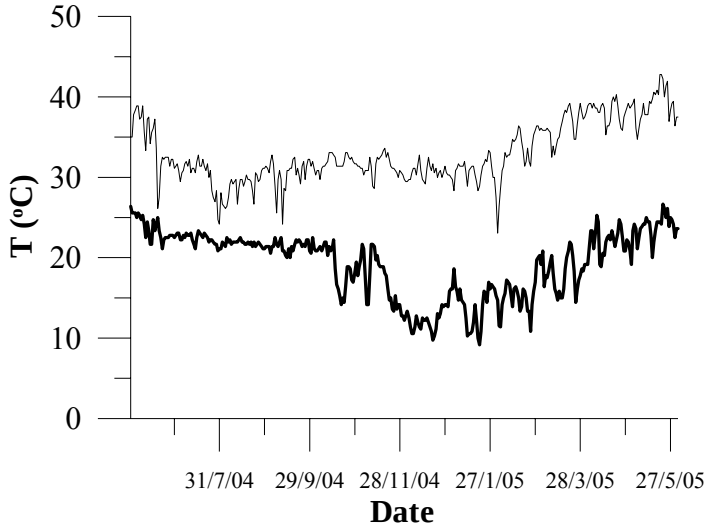

Figure 30: Average daily maxium and minium temperature

[8] http://www.iwmi.cgiar.org/WAtlas/atlas.htm
[9] http://www.wunderground.com

6.4.3 Relative humidity

Public domain data[9] are used for daily relative humidity.

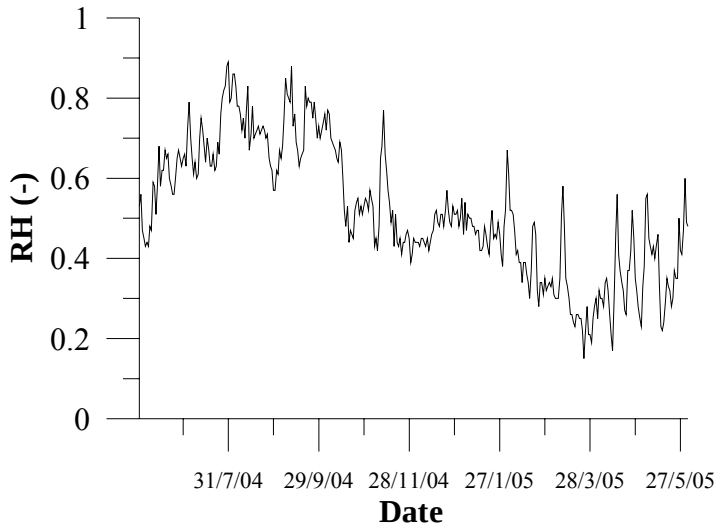

Figure 31: Average daily relative humidity

6.4.4 Wind speed

Public domain data[9] are used for wind speed.

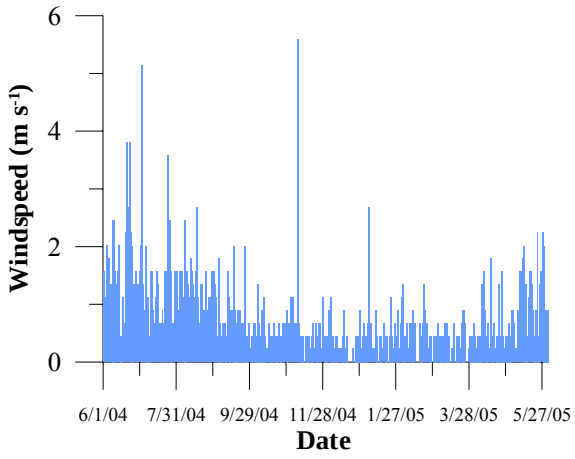

Figure 32: Average daily windspeed

6.4.5 Precipitation

Because of the spatial variation in precipitation a different approach has been adopted. The TRMM precipitation rasters as described in Chapter 5 are used to generated monthly precipitation for each sub basin from October 2004 to September. At the center of each sub basin a virtual meteorological station is generated. The monthly precipitation data are converted to daily values using the following procedure:

- A random day in the month is selected.
- A random amount of precipitation is generated. In the monsoon months (June, July, August, September) this amount is between 30 and 60 mm day^{-1}. In all other months this amount is between 10 and 20 mm day^{-1}.
- This process is repeated until the total amount of monthly precipitation is distributed.

An example of the daily precipitation of two sub basins is given in Figure 33. Sub basin 57 is located in the Western ghats in the south western part of the catchment and sub basin 61 is located in the eastern part of the catchment.

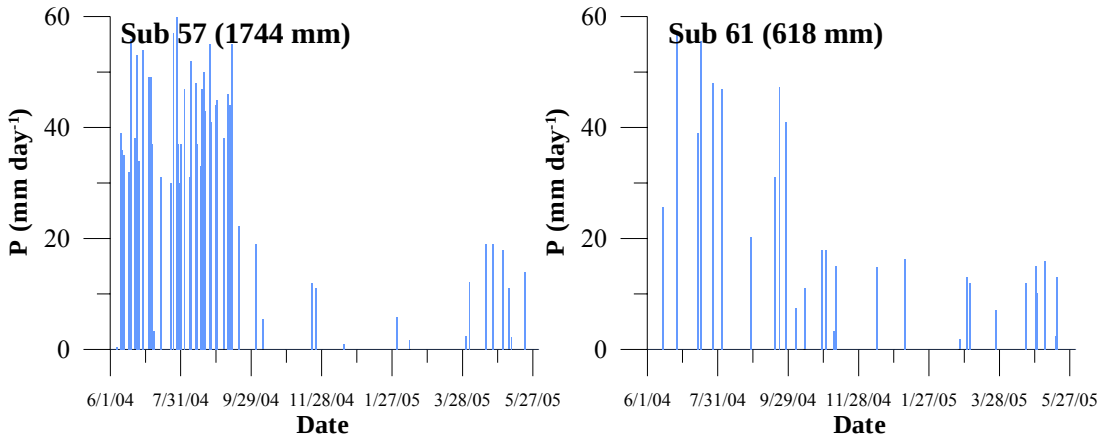

Figure 33: Daily precipitation for sub basins 57 and 61

6.5 Management practices

Quantifying the impact of land management and land use on water supply and quality is a primary focus of environmental modeling. SWAT allows very detailed management information to be incorporated into a simulation. In the model for the Upper Bhima catchment the following operations are used:

- The plant operation initiates plant growth. This operation can be used to designate the time of planting for agricultural crops or the initiation of plant growth in the spring for a land cover that requires several years to reach maturity (forests, orchards, etc.). The plant operation will be performed by SWAT only when no land cover is growing in an HRU. Before planting a new land cover, the previous land cover must be removed with a kill operation or a harvest and kill operation. Information required in the plant operation includes the timing of the operation (month and day or fraction of base zero potential heat units), the total number of heat units required for the land cover to reach maturity, and the specific land cover to be simulated in the HRU.
- The harvest and kill operation stops plant growth in the HRU. The fraction of biomass specified in the land cover's harvest index (in the plant growth database) is removed from the HRU as yield. The remaining fraction of plant biomass is converted to residue on the soil surface.

- The fertilizer operation applies fertilizer or manure to the soil. Information required in the fertilizer operation includes the timing of the operation (month and day or fraction of plant potential heat units), the type of fertilizer/manure applied, the amount of fertilizer/manure applied, and the depth distribution of fertilizer application.
- Application of irrigation water. Information is required on the amount of irrigation water to be applied, the salt content of the irrigation and the timing of the operation.

The agricultural land use classes need to be parameterized for different crops and management activities such as fertilization and irrigation. As described in chapter 3 three agricultural land use classes have been defined, which have been parameterized as follows:

Table 6: management operations rainfed agriculture (AGR1)

Date	Crop	Operation	Remarks
Jun-10	Sorghum	Planting of crop	
Jun-22	Sorghum	Fertilizer application	300 kg/ha Urea
Sep-30	Sorghum	Harvest	

Table 7: management operations supplemental irrigated agriculture (AGR2)

Date	Crop	Operation	Remarks
Jun-10	Sorghum	Planting of crop	
Jun-10	Sorghum	Fertilization	300 kg/ha Urea
Aug-01	Sorghum	Fertilization	300 kg/ha Urea
Sep-29	Sorghum	Harvest	
Oct-15	Winter wheat	Planting of crop	
Oct-17	Winter wheat	Fertilization	300 kg/ha Urea
Nov-01	Winter wheat	Fertilization	300 kg/ha Urea
Nov-10	Winter wheat	Irrigation	40 mm
Nov-20	Winter wheat	Irrigation	40 mm
Dec-15	Winter wheat	Irrigation	100 mm
Jan-15	Winter wheat	Irrigation	100 mm
Feb-10	Winter wheat	Fertilization	300 kg/ha Urea

Table 8: management operations intensive irrigated agriculture (AGR3)

Date	Crop	Operation	Remarks
Jun-02	Sugarcane	Planting of crop	
Jun-02	Sugarcane	Fertilization	300 kg/ha Urea
Jun-15	Sugarcane	Irrigation	60 mm
Jul-15	Sugarcane	Irrigation	40 mm
Aug-15	Sugarcane	Irrigation	50 mm
Sep-01	Sugarcane	Fertilization	300 kg/ha Urea
Sep-15	Sugarcane	Irrigation	20 mm
Oct-15	Sugarcane	Irrigation	50 mm
Nov-15	Sugarcane	Irrigation	40 mm
Dec-15	Sugarcane	Irrigation	40 mm
Jan-01	Sugarcane	Fertilization	300 kg/ha Urea
Jan-15	Sugarcane	Irrigation	40 mm
Feb-15	Sugarcane	Irrigation	50 mm
Mar-15	Sugarcane	Irrigation	100 mm
Apr-15	Sugarcane	Irrigation	100 mm
May-15	Sugarcane	Irrigation	100 mm
May-30	Sugarcane	Harvest	

6.6 *Reservoirs*

The upper Bhima catchment is a complex catchment and stream flow is for a large part determined by reservoirs in the upstream area of the catchment which receives most precipitation. Data on reservoirs is scarce and sensitive given the water disputes between the different states. A total of 13 reservoirs have been modeled in SWAT. The actual reservoirs and the locations of the reservoirs in the model are shown in Figure 34. SWAT locates the reservoirs for routing purposes on the sub basin boundary. In the model a user specified release rate is used to model outflow out of the reservoir. Besides monthly releases the following inputs are required for each reservoir:

- RES_ESA: Surface area of the reservoir when filled to the emergency spillway (ha)
- RES_PSA: Surface area of the reservoir when filled to the principal spillway (ha)
- RES_EVOL: Volume of water held in the reservoir when filled to the emergency spillway (10^4 m^3 H_2O)
- RES_PVOL: Volume of water held in the reservoir when filled to the principal spillway (10^4 m^3 H_2O)
- RES_VOL: Initial Volume of water held in the reservoir when filled at the beginning of the simulation (10^4 m^3 H_2O)

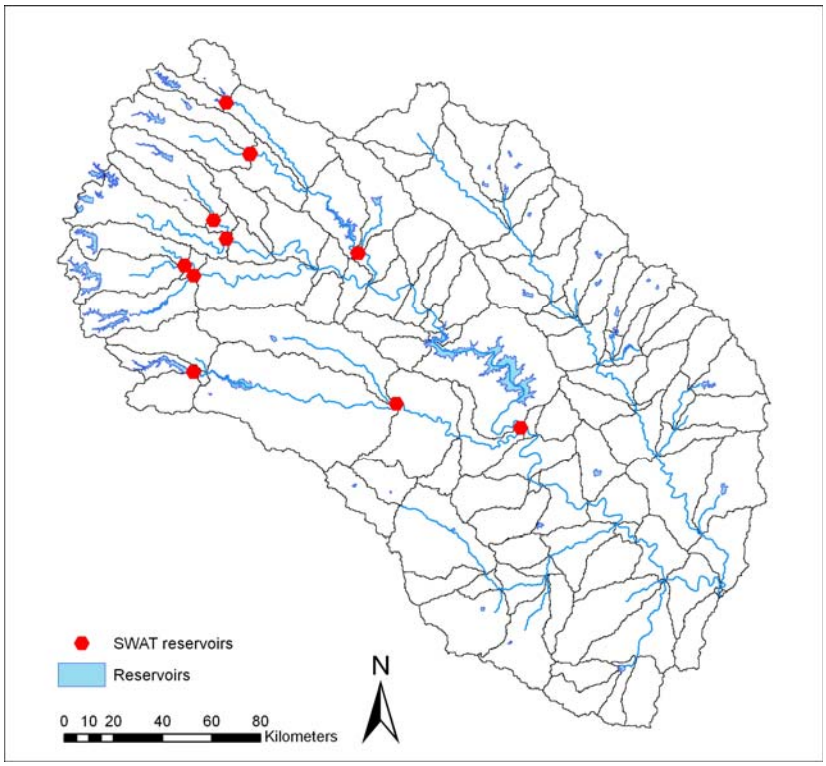

Figure 34: Location of reservoirs

For modeling purposes the reservoirs are grouped together into two reservoirs; one for the Ujani branch in the middle and one for the Bhatghar branch in the south. It is assumed that all areas with AGR3 land use receive their irrigation water directly from the reservoirs. The irrigation year 2004-2005 is an average year and it is assumed that the irrigation amounts specified in Table 8 are actually required. The required stream flow to fulfill these irrigation requirements for both branches are shown in Figure 38.

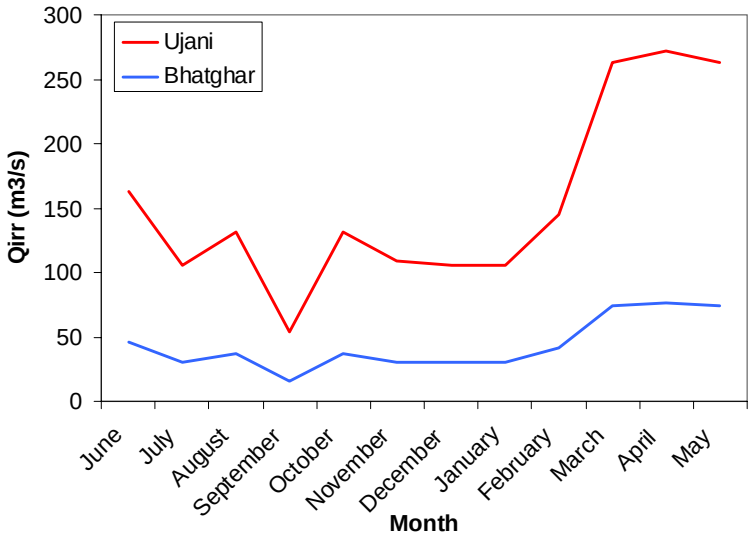

Figure 35: Stream requirements to fullfill irrigation requirements

The difference between the amount of water that flows into the reservoirs and the amount that is required for irrigation is released as stream flow to downstream basins. The distribution across the different months is based on the historical monthly stream flow distribution presented in.

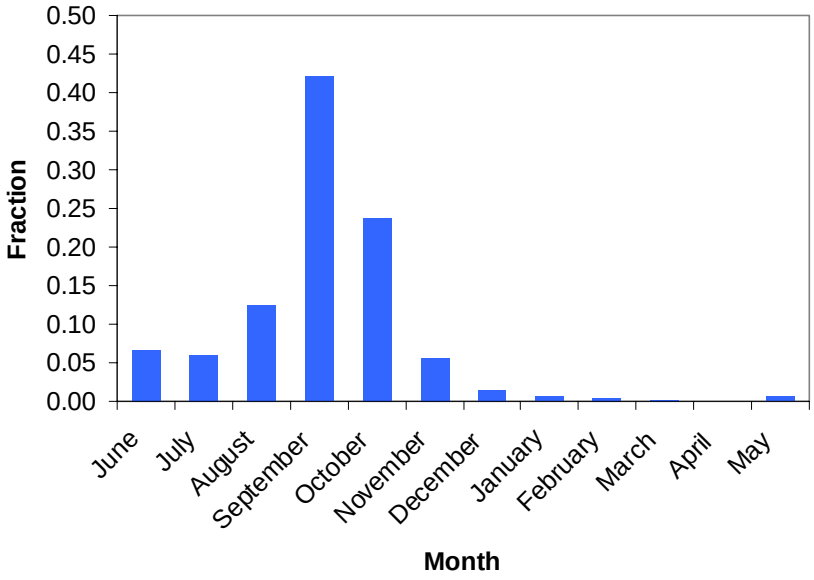

Figure 36: Monthly fractions of annual streamflow

7 Sensitivity analysis

Major objective of the project is to use the spatial patterns of ET in the auto calibration of the SWAT model. The model independent parameter estimation package PEST will be used for this purpose (Doherty, 2004).

The purpose of PEST (which is an acronym for Parameter ESTimation) is to assist in data interpretation, model calibration and predictive analysis. Where model parameters and/or excitations need to be adjusted until model-generated numbers fit a set of observations as closely as possible then, provided certain continuity conditions are met, PEST should be able to do the job. PEST will adjust model parameters and/or excitations until the fit between model outputs and laboratory or field observations is optimised in the weighted least squares sense. Where parameter values inferred through this process are nonunique, PEST will analyse the repercussions of this nonuniqueness on predictions made by the model.

The first step in setting up PEST is however to define a logical set of parameters and observation which are to be used in the optimization. Using a spatial set-up results in a number of new challenges. The SEBAL analysis provides an eight month time series with a biweekly time step of both reference and actual ET. SWAT provides a 12 month monthly time series of reference ET (ET_{ref}) and actual ET (ET_{act}) per HRU. The parameter optimization is performed on actual ET. The SEBAL data are first aggregated to monthly data and summarized per HRU in order to be able to directly compare model outputs to the SEBAL analysis. Before setting up PEST there are two topics which need to be addressed:

- There is a need to explore whether the reference ET generated by SEBAL and SWAT is similar in time and space and if not a simple manual calibration will need to be performed. Since ET_{ref} is the basis for the calculation of ET_{act} and it is very important that the observed and modeled ET_{ref} time series per subbasin are similar before embarking on any optimization effort with PEST.
- Secondly we need to know if there are significant relations ships between the difference in observed ET_{act} and modeled ET_{act} (ΔET_{act}) and time, land use type, soil type, water management and topography. Before selecting the parameters we would like to optimize we need to know which part of the system can explain the ΔET_{act} in both time and space.

These two topics are described in this chapter.

7.1 *Exploration of reference evapotranspiration*

The reference evapotranspiration is only affected by climatic parameters and can be computed by weather variables only and is valid for the hypothetical reference crop under well watered conditions (Allen et al., 1998). The meteorological data for Pune and Sholapur are used for this purpose both in SWAT and in SEBAL. Conceptually ET_{ref} in SWAT is calculated per sub-basin, because it only depends on the meteorological data and not on soil and land use characteristics.

There are differences in space and time in ETref between SEBAL and SWAT mainly caused by spatial altitude dependent operations which SEBAL performs on important parameters. The DEM is used to calculated and correct air pressure and density and thus the psychometric constant. The DEM is also used to correct the absorbed solar radiation values, both for slope and aspect. Southern facing terrain due to the angle of incidence, absorb more solar radiation per unit land than the Northern facing slope. Another cause of this difference is the fact that SEBAL uses grass (0.12m height) as a reference crop and SWAT uses alfalfa (0.40m height).

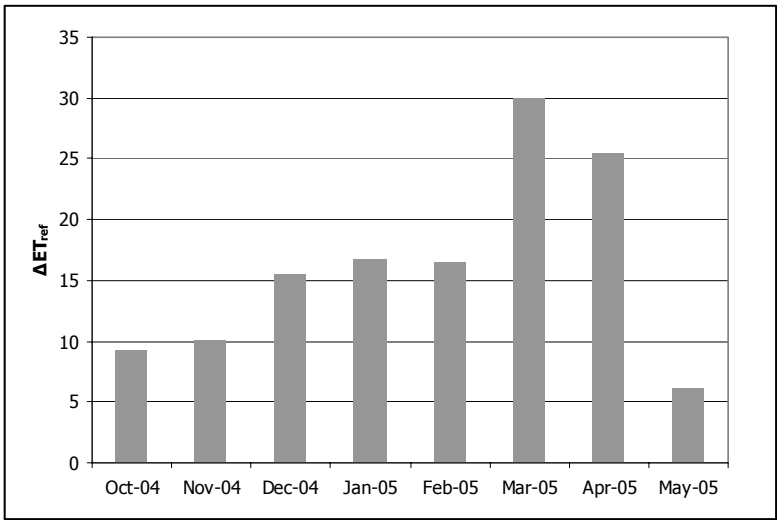

Figure 37: Monthly difference in ET_{ref} between calibrated and uncalibrated model

Figure 37 shows the monthly difference in ET_{ref} for the entire Upper Bhima catchment. Summed over a year these differnce may accumulate to over 150 mm annualy. To overcome these differences a simple calibration procedure has been applied and the amount of incident solar raditation has been correccted per subbasin per month to calibrate the ET_{ref}. Assuming a lineair relation between solar raditaion and ET_{ref} the correction factors have been derived iteratively. The largest correction is required in the month March (average = 6.1%) and the smallest in May (average = 1.1%). Figure 38 shows the scatterplot of the uncalibrated and calibrated annual ET_{ref} per subbasin. Calibrated SWAT ET_{ref} exhibits perfect correlation with SEBAl ET_{ref}.

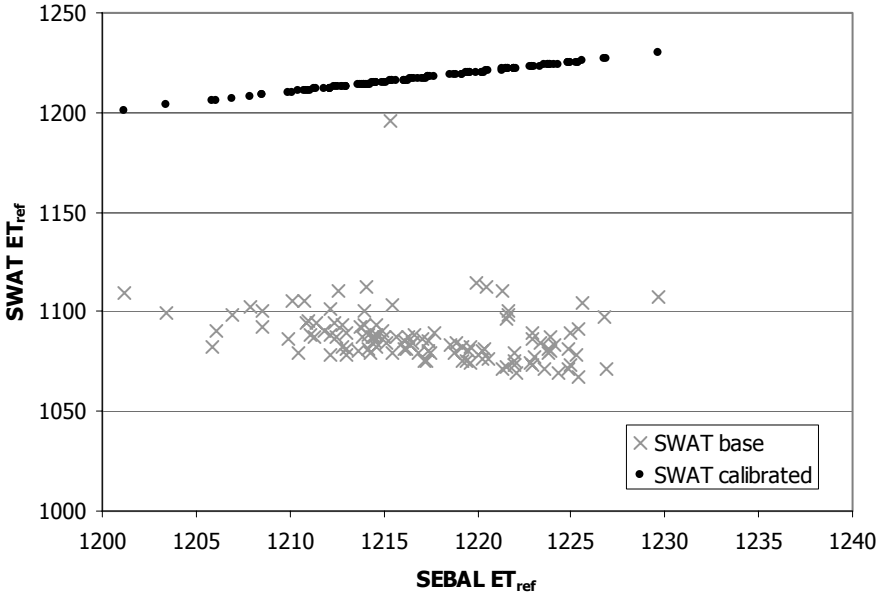

Figure 38: uncalibrated and calibrated sum of ET_{ref} from October 2004 to May 2005 per SWAT subbasin

7.2 Differences in acual evapotranspiration

After calibration of ET_{ref} it is visually verified through a set of box whisker plots whether ΔET_{act} (ET_{act} SEBAL – ET_{act} SWAT) is explained by different land use, different soil type, month, or precipitation zone. This analysis leads to the identification of a number of PEST optimisation runs.

Figure 39 shows box-whisker plots of monthly ΔETact per land use, soil type, month and precipitation class respectively. The order of magnitude of SWAT ETact is similar to SEBAL, ΔETact is on average slightly positive indicating that ETact measured by SEBAL is slightly higher than SWAT simulated values. The distribution of ΔETact resembles a normal distribution in most cases, but ranges between the first and third quartile are considerable and vary between land uses, soil types, months and precipitation classes.

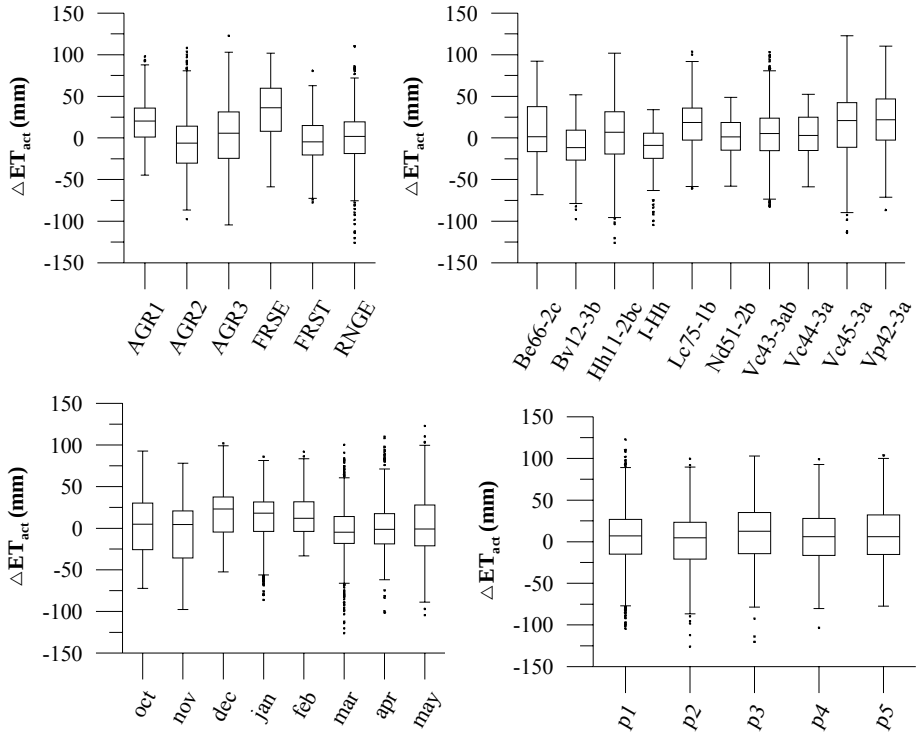

Figure 39: Box whisker plots of monthly ΔET_{act} (SEBAL – SWAT) per land use class (top left), soil class (top right), month (bottom left) and precipitation class (bottom right; p1 = 0-800 mm yr^{-1}, p2 = 800-1100 mm yr^{-1}, p3= 1100-1400 mm yr^{-1}, p4=1400-1700 mm yr^{-1}, p5=1700-2000 mm yr^{-1})

There are clear differences between land uses, soil type and month. The differences between the precipitation classes are less pronounced. This led to the formulation of the following optimisation runs:

Available water capacity (AWC). The AWC is defined as the difference between the field capacity of the soil and the permanent wilting point. It is defined per soil layer per soil type and determines to a large extent the water buffer capacity of the soil. Ten different soil types with two layers each lead to 20 different parameters to be optimized.

Maximum potential leaf area index (BLAI). The LAI is the leaf area divided by the land area. The BLAI is one of six parameters that determine leaf area development of a crop in SWAT and determines the maximum threshold. BLAI is specified per land use type, with the exclusion of water surfaces this lead to 6 parameters to be optimized (**Error! Reference source not found.**).

Monthly rainfall increment (RFINC). The RFINC is specified per month and per sub basin and is defined as the relative monthly adaptation in rainfall. The assumption is made that the spatial distribution of the TRMM derived precipitation is correct, however that for specific months relative corrections are allowed within clear boundaries. This leads to one variable to be optimized per month.

Groundwater revap coefficient (REVAP1 and REVAP2). In SWAT water may conceptually move from the shallow aquifer into the overlying unsaturated zone. In dry periods water is evaporated from the capillary fringe is evaporated and this process is referred to as groundwater revap and is in SWAT

quantified by the revap coefficient (βr) multiplied by ETref. Two optimisation runs are designed. For the first optimisation run one βr for each land use, except water, is defined (REVAP1, 6 variables). For the second optimisation run it is assumed that βr varies per land use and per elevation zone. Four different elevation zones are defined (0-500 m, 500-600 m, 600-700m and >700m). In combination with land use this results in 21 unique βr resulting from unique combinations of elevation zone and land use class (REVAP2, 21 variables)

8 Calibration

8.1 Results

All optimisation runs calculate the Φ based on monthly data at sub basin level. In total there are 920 observations (8 months times 115 sub basins). Two final optimisation runs are performed based on the results of the individual runs (COM1 and COM2). COM1 combines AWC, RFINC and GWREVAP and COM2 combines AWC, RFINC and GWREVAP2.

Table 9: Results of different optimisations runs. #var and #obs are the number of variables and observations used in the optimisations. The RMSE (Φ) is the Root Mean Square Error or objective function, ε is the average of the residuals and # model calls is the number of model calls required to reach the optimisation results.

PEST run	Variable	# var	# obs	RMSE (Φ)	r^2	ε (mm)	# model calls
BASE	-	0	920	5.29E+05	0.40	5.20	-
AWC	Available water content	20	920	4.49E+05	0.49	5.90	664
BLAI	Maximum plant leaf area index	6	920	5.19E+05	0.41	5.50	68
RFINC	Monthly rainfall increment	12	920	2.54E+05	0.70	0.80	324
GWREVAP	Groundwater revap coefficient	6	920	2.78E+05	0.68	1.60	55
GWREVAP2	Groundwater revap coefficient	21	920	2.66E+05	0.70	1.70	792
COM1	Available water content, monthly rainfall increment, groundwater revap coefficient	53	920	1.63E+05	0.81	0.50	2987
COM2	Available water content, monthly rainfall increment, groundwater revap coefficient	38	920	1.77E+05	0.79	-0.45	1610

Table 9 shows the results for the different optimisation runs. It shows that the monthly rainfall increments and the groundwater revap coefficient have the largest effect on the RMSE. Variation of BLAI has the least effect and only increased r2 by 0.01, which is negligible. The best results are achieved by combining optimisation runs AWC, RFINC, GWREVAP2. The RMSE is reduced by 69% and the r2 is 0.81. This means that 81% of the variation in monthly ETact for all 115 sub basins is explained by the optimised model. COM2 results do not deviate significantly from COM1 results. However the number of variables used in the optimisation, 38 versus 53, results in a much lower number of required model calls (1610).

There are several ways to evaluate the reliability of any optimisation of a distributed hydrological model across time and space. Figure 40 the scatter plots for COM1 between SEBAL ETact and SWAT ETact on catchment, sub basin and HRU level respectively. It also shows the individual monthly data and the eight month sum of ETact. The figure shows that the goodness of fit decreases with spatial and temporal detail. The r2 of monthly catchment ETact for example is as high as 0.90, while at HRU level the r2 is only 0.35. In time we see similar patterns. The r2 at monthly sub basin level is 0.81 while if the eight month sum is analyzed the r2 increase to 0.92.

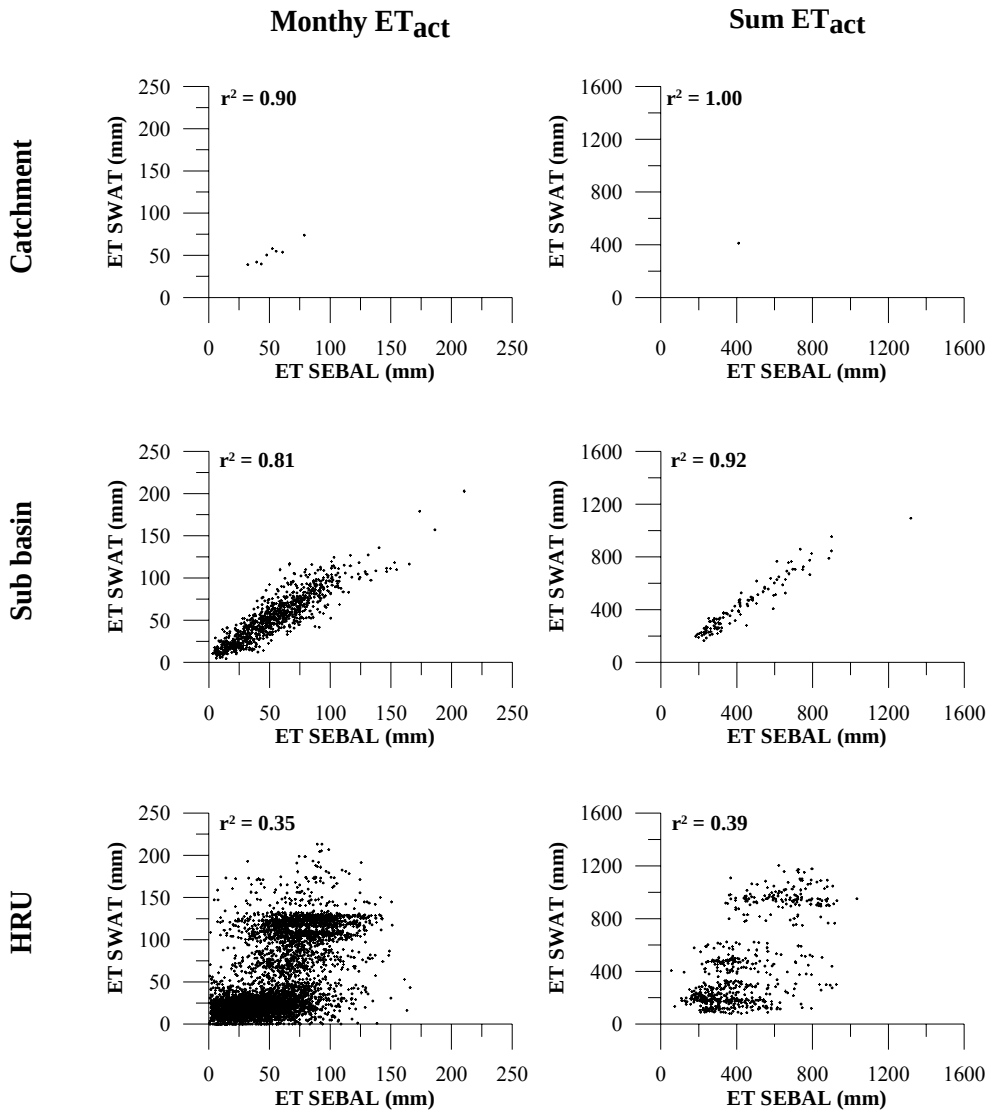

Figure 40: Scatter plots of SEBAL and SWAT $ET_{act.}$ Monthly data are shown on the left side graphs and the eight month sum is on the right side of the graphs. Spatial detail increases from top to bottom and ranges from catchment, sub basin to HRU level respectively. SWAT results relate to COM2 optimisation.

Figure 41 shows the map with the eight month ETact sum for SWAT and SEBAL at sub basin and at HRU level. At sub basin level the spatial patterns between SWAT and SEBAL are highly consistent. At HRU level there are considerable differences. The general spatial patterns are well depicted however some HRUs within a sub basin evaporate more than measured with SEBAL and some less, however aggregated over the entire sub basin these differences are levelled out.

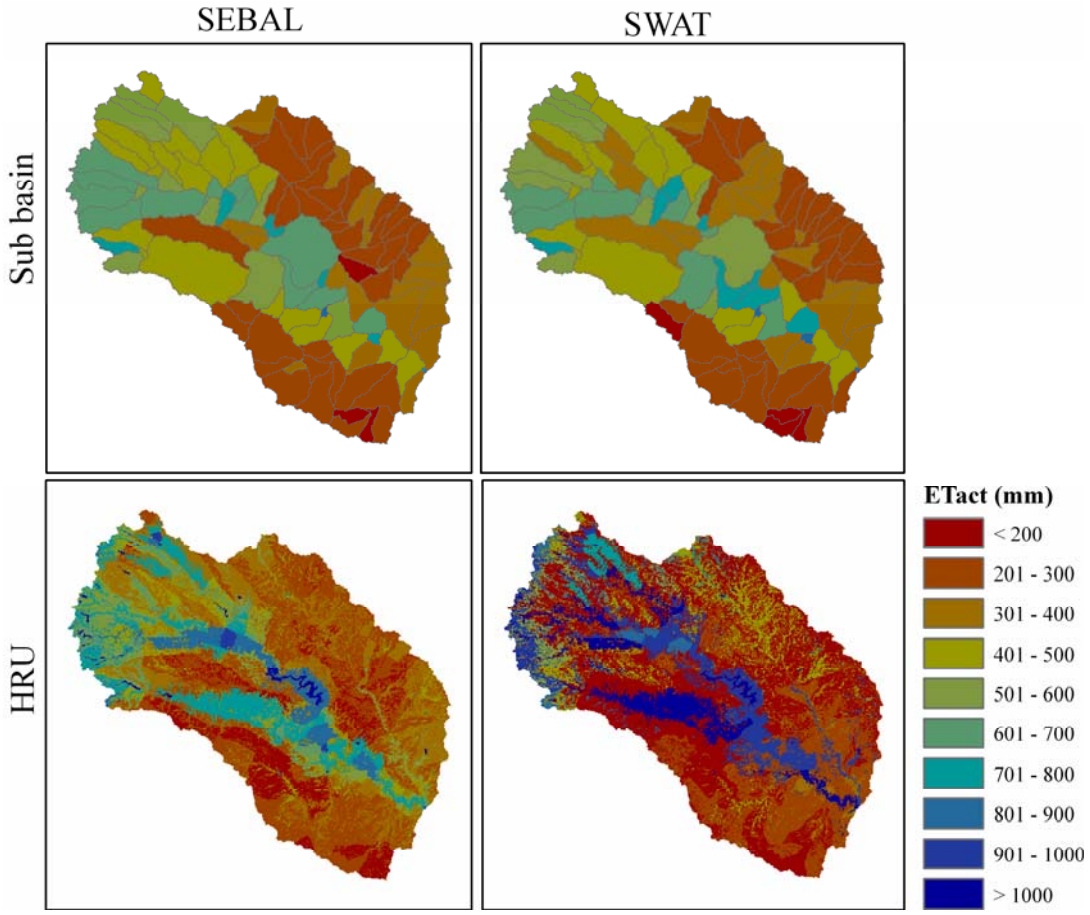

Figure 41: Eight month sum of ET_{act} for SWAT and SEBAL on sub basin and HRU level respectively. SWAT results relate to COM2 optimisation.

We have shown that it is possible to accurately predict monthly ETact at sub basin level the results are verified by cross checking the discharges in the river system. No measured discharged are available for the simulation period (June 2004 – May 2005). There is however a dataset available from 1970 to 1996. The discharges of the Sina tributary are used, because the Sina catchment is less disturbed by large reservoirs and man made structures than the Bhima tributary.

Table 10 shows the observed and simulated discharges. The simulated discharges in 2004-2005 are well within one standard deviation of the average measured discharges between 1970 and 1996. It should be noted though hat the coefficient of variation in the observed discharges are large ranging from 68% in August to 170% in March.

Table 10: Discharges Sina branch. Q_{swat} is the modelled dischare from june 2004 to may 2005. Q_{obs} is the average observed discharge from 1970-1996 and CV_{obs} is the coefficient of variation in the observed discharges.

Month	Q_{SWAT} (m^3/s)	Q_{obs} (m^3/s)	CV_{obs} (%)
june	4	90	161
july	240	540	96
august	366	740	68
september	456	562	81
october	78	297	114
november	47	61	117
december	45	28	112
january	16	15	98
february	9	8	97
march	2	5	170
april	0	3	149
may	0	6	149

8.2 Discussion and conclusions

The spatial distributed hydrological model SWAT can be successfully calibrated using the GML algorithm on the basis of Remotely Sensed derived evapotranspiration in a data scarce area. The best results were obtained by optimising a combination of soil, meteorological and groundwater related parameters on an eight month time series of sub basin actual evapotranspiration. Optimising a total of 53 variables using 920 monthly observations increased the r2 from 0.40 to 0.81. A validation with measured discharges reveals that the modelled discharges are well with the one standard deviation of the observed data.

Separate optimisation runs revealed that ETact is more sensitive to the groundwater and meteorological parameters than the soil and land use parameters. On sub basin level the ETact shows least response to the land cover dependent maximum leaf area index.

A first important step when calibration on ETact is to ensure that ETref is optimised first. We show that a near perfect match between observed and measured ETref by small adaptations (average = 3.5%) of monthly radiation.

It is also concluded that at the HRU level more work is required to fine-tune the calibration procedure. The calibration is only reliable at the spatial and temporal scale on which the observations, used in the optimisation, are based. Future work should focus on calibration strategy that incorporates HRU level ETact observations and discharges at a high temporal resolution in the objective function.

Recently interest in using simulation models in ungauged or sparsely gauged basins has increased leading to some concerted actions. The most relevant is the Prediction in Ungauged Basin (PUB) initiative; an International Association for Hydrological Sciences (IAHS) initiative for the decade of 2003-2012, aimed at uncertainty reduction in hydrological practice (Sivapalani et al., 2003). PUB

focuses the development of new predictive approaches that are based on "understanding" of hydrological functioning at multiple space-time scales. This study provides an ET based innovative approach at different temporal and spatial scale that fits well into PUBS science program.

Differences in space and time in ETref between SEBAL and SWAT are caused by spatial altitude dependent operations which SEBAL performs on important parameters. The DEM is used to calculated and correct air pressure and density and thus the psychometric constant. The DEM is used to correct the absorbed solar radiation values, both for slope and aspect. Southern facing terrain due to the angle of incidence, absorb more solar radiation per unit land than the Northern facing slope. Another cause of this difference is the fact that SEBAL uses grass as a reference crop and SWAT uses alfalfa.

Traditional calibration on a limited number of discharge stations lumps all hydrological processes together and chances on the equifinality problem are much larger. In this study we show that using spatially distributed observations with a monthly temporal resolution provide much better results. The success of the approach lays in the spatial and temporal isolation of the calibration problem at hand. Information content of a time series of discharges at the outlet of a catchment is simply insufficient to attribute deviations between observation and simulation to specific processes at a specific location at a specific point in time. Although we have found very good results at the sub basin level on a monthly time step, more work is required to increase the reliability of the results at HRU level and eventually with a daily time step. Promising in this respect could be the use of a combined objective function including both spatial evapotranspiration and discharges at a high temporal resolution.
One of the variables used in the optimisation is a monthly rainfall increment. It is generally not common practice to vary model excitations in a calibration procedure, however we believe that in this case it is legitimate within tight bounds, since precipitation is acquired with TRMM and subject to larger errors than station data.

In this study the GML algorithm was used in the optimisation and there are no indications that optimisations did not converge into a global minima. The main cause is probably that a time series of spatial ET exhibits more linear behaviour than discharge at a limited number of locations. Moreover it has been shown that global search algorithms require much more function calls to identify the global minimum. The GML algorithm is much more efficient in this respect (Skahill and Doherty, 2006). Given the fact that the best optimisation in this study required 2987 model calls this is a critical requirement.

9 Results

9.1 Water balances

9.2 Biomass and crop production

9.3 Scenarios

10 Conclusion

11 References

Allen, R., Pereira, L.A., Raes, D., Smith, M., 1998, Crop evapotranspiration; guidelines for computing crop water requirements, FAO Irrigation and Drainage Paper No. 56, FAO, Rome

Bastiaanssen, W.M.A., Klaasse, A., Zwart, S., Immerzeel, W. and Droogers, P., 2006, The hydrological flow path and options for sustainable water resources management in the overexploited Rio Bravo Basin: A preliminary analysis from remote sensing and hydrological modeling, WaterWatch report, Wageningen

Brutsaert, W. and M. Sugita, 1992. Application of self preservation in the diurnal evolution of the surface
energy balance budget to determine daily evaporation, J. Geophys. Res. 97(D17): 18377-18362

Crago, R.D., 1996. Conservation and variability of the evaporative fraction during the daytime, J. of Hydr. 180: 173-194

Doherty, J., 2004, PEST; Model-Independent Parameter Estimation; User Manual: 5th edition. Watermark Numerical Computing

Farah, H.O., 2001. Estimation of regional evaporation under different weather conditions from satellite and meteorological data, Ph.D. thesis, Department of Agrohydrology, Wageningen University, The Netherlands: 170 pp.

FAO, 1974. FAO-Unesco Soil Map of the World, 1:5.000.000. Unesco, Paris.

FAO, 1995. FAO-Unesco digital Soil Map of the World and derived soil properties, 1:5.000.000. Unesco, Paris.

Franke R. 1982. Smooth Interpolation of Scattered Data by Local Thin Plate Splines. Comp. & Maths. with Appls. 8: 237-281.

Hargreaves, G.L., G.H. Hargreaves, and J.P. Riley. 1985. Agricultural benefits for Senegal River Basin. J. Irrig. and Drain. Engr. 111(2):113-124.

Hooghoudt, S.B. 1940. Bijdrage tot de kennis van enige natuurkundige grootheden van de grond. Versl. Landbouwkd. Onderz. 46: 515-707.

Immerzeel, W.W. and Droogers, P., 2005, Exploring evaporation reduction in the Hai basin; analysis using the SWAT model, FutureWater report, Wageningen

Lillesand, T.M. and Kiefer, R.W., 2000, Remote Sensing and Image Interpretation, 4th edition, John Wiley & Sons, New York

Monteith, J.L. 1965. Evaporation and the environment. p. 205-234. In The state and movement of water in living organisms. 19th Symposia of the Society for Experimental Biology. Cambridge Univ. Press, London, U.K.

Neitsch, S.L., Arnold, J.G., Kiniri, J.R., Williams, J.R., 2001, Soil and Water Assessment Tool Theoretical Documentation Version 2000. Texas: Grassland, Soil and Water research Laboratory and Blackland Research Center.

Nicols, W.E. and R.H. Cuenca, 1993. Evaluation of the evaporative fraction for the parameterization of the surface energy balance, Water Resources Research 29(11): 3681-3690 NOAA National Weather Service, West Gulf River Forecats Center.

Priestley, C.H.B. and R.J. Taylor. 1972. On the assessment of surface heat flux and evaporation using large-scale parameters. Mon. Weather Rev. 100:81-92.

Ritchie, J.T. 1972. A model for predicting evaporation from a row crop with incomplete cover. Water Resour. Res. 8:1204-1213.

Shuttleworth, W.J., R.J. Gurney, A.Y. Hsu and J.P. Ormsby, 1989. FIFE: the variation in energy partitioning at surface flux sites, IAHS Publ. 186: 67-74

Sivapalani M, Takeuchi K, Frank SW, Gupta VK, Karambiris H, Lakshmi V, Liang X, McDonell JJ, Mendiondo, EM, O'Conell PE, Oki T, Pomeroy JW, Schertzer D, Uhlenbrook S, Zehe E. 2003. IAHS Decade on Predictions in Ungauged Basins (PUB), 2003–2012: Shaping an exciting future for the hydrological sciences. Hydrological Sciences 48: 857-880

Skahill BE, Doherty J. 2006. Efficient accommodation of local minima in watershed model calibration. Journal of Hydrology (in press).

Smedema, L.K. and D.W. Rycroft. 1983. Land drainage—planning and design of agricultural drainage systems, Cornell University Press, Ithica, N.Y.

Tucker, C.J., 1979, Red and photographic infrared linear combination for monitoring vegetation. Remote Sensing of Environment, 8, 127-150